

Dimensional Reduction of Lattice Gauge Theory in (2+1) dimensions

Dissertation zur Erlangung des Doktorgrades
vorgelegt von
Konstantin Petrov

November 14, 2018

Contents

1	Reducing the degrees of freedom	5
1.1	The Model	5
1.2	Naive reduction	7
1.3	Classical reduction	8
2	Dimensional reduction	11
2.1	Perturbation Theory	11
2.2	Action	13
2.3	Simulations	16
2.4	Polyakov loop correlations and Masses	19
2.4.1	Comparison with the original model	19
2.4.2	Scaling test	21
2.4.3	Screening Lengths	25
2.5	Spatial Wilson loop	28
3	Reduced Model Per Se	33
3.1	Phase structure of the model	33
3.2	The spectrum of the model	38
3.3	Weak “Strong” Interactions Between Colorless States	45
3.3.1	Weak Residual Interactions: The A -fields condensates	45
3.3.2	Weak Residual Interactions: Properties of the Correlations	46
4	$Z(3)$ symmetric action	55
5	Conclusions and outlook	59
6	Acknowledgements	63
A	Appendix	65
A.1	General $SU(3)$ formulae and definitions	65
A.2	One Link Integral	67
A.3	One-loop Feynman diagrams for the vacuum polarization	70

A.4	Free field theory	76
A.5	Weak field expansion for Polyakov loops	79
A.6	Factorization of Matterfields	81

Introduction

During last decades quantum chromodynamics (QCD), as a part of the Standard Model, established itself as a working theory of the strong interactions. We believe that quarks and gluons are the basic objects that make up the hadronic matter. This theory has been very successful in predicting phenomena involving large momentum transfer. Unfortunately, its direct applications are limited to this particular case, when the coupling constant is small and perturbation theory is reliable. However, in the hadronic world, the coupling constant is of the order of one and the perturbation series do not converge. In this domain the discrete space-time formulation of quantum chromodynamics provides a non-perturbative tool for the calculation of the hadronic spectrum and basically every other observable from first principles. Lattice QCD was used to study the questions of confinement and chiral symmetry breaking.

Lattice QCD is usually formulated on a square Euclidean space-time grid. No new parameters or field variables are involved in this formulation, hence, it retains the fundamental character of QCD. In fact, it can serve two purposes. First, it acts as a non-perturbative regularization scheme. At finite values of the lattice spacing a , which provides an ultra-violet cutoff there are no infinities (as long as lattice is finite itself). On the other hand it gives us an ability to do direct simulations of lattice QCD on the computer using methods analogous to those used in statistical mechanics. One can in principle calculate all correlation functions of hadronic operators and matrix elements of any operator between hadronic states. These simulations are based on a Monte Carlo integration of the Euclidean path integral and have therefore both discretization and statistical errors.

The starting point for lattice QCD is the partition function in Euclidean space-time

$$Z = \int \mathcal{D}A_\mu \mathcal{D}\psi \mathcal{D}\bar{\psi} e^{-S} \quad (1)$$

where S is the QCD action

$$S = \int d^4x \left(\frac{1}{4} F_{\mu\nu} F^{\mu\nu} - \bar{\psi} \mathcal{M} \psi \right) \quad (2)$$

Here \mathcal{M} is Dirac operator, fermions are represented through Grassmann variables ψ and $\bar{\psi}$; $F_{\mu\nu}$ is the Yang-Mills field strength tensor for gauge fields A_μ , which are elements of the $SU(3)$ algebra. Fermion fields can be then integrated

out exactly, leaving us with

$$Z = \int \mathcal{D}A_\mu \det \mathcal{M} e^{-S_G} \quad (3)$$

The partition function is now an integral over background gauge configurations. The fermionic contribution is contained only in the very non-local term $\det \mathcal{M}$. The model defined so describes zero temperature physics. To calculate the thermodynamical quantities at finite temperature one has to make the time direction periodic and set its length to be the inverse temperature. We write then

$$S = \int_0^{1/T} dx_0 \int_V d^3x \left(\frac{1}{4} F_{\mu\nu} F^{\mu\nu} - \psi \mathcal{M} \bar{\psi} \right) \quad (4)$$

where x_0 refers to the time coordinate and V is the physical volume of the system. The gauge fields have then periodic boundary conditions and fermion fields - anti-periodic ones.

The fermionic determinant is the major complication in all simulations on the lattice, due to its non-locality and other technical details. The model without this term, so-called pure gauge theory, has been in the focus of the interest for many years. It was successfully simulated by several groups [6] and the equation of state and the phase diagram were successfully studied and extrapolated to continuum

The full model, however, suffers from severe problems of both calculational and theoretical type. Despite significant progress during last years [5], the time estimated for the continuum extrapolation of the results from the direct simulations of any of the existing fermionic actions (aiming, e.g. at the determination of the quark masses) varies from several to hundred teraflops-years. Thus one would want to have an indirect method of calculating the quantities of interest, which would require significantly less computer time. One of such methods, applicable at high temperatures, is the so-called dimensional reduction ([7]-[11]). In general it is a method of turning (D+1)-dimensional system at high temperature into the D-dimensional one. Using the fact that at high temperature the domain of integration in (4) shrinks one can perturbatively get rid of the non-static time-like degrees of freedom. Such an effective model is much cheaper to simulate and is supposed to reproduce the long-distance behavior of the model. This method was successfully applied to QCD at high temperature and to the study of the electro-weak transition. At the same time the domain of its validity is not well-studied, and this is the primary aim of the current work.

We focus on the (2+1)-dimensional pure gauge field theory, which is then reduced to a two-dimensional one. The source model does not include the dynamic fermions and can be simulated with a high precision using the present

computer power. While being different from the standard (3+1)-dimensional system it shares with it many important properties, like static quark confinement; the infrared singularities are even more severe. The reduced model can be simulated even on personal computers.

Current work is organized as follows. In the first chapter we define our model and operators of interest and review simple models of the dimensional reduction. In the second one we present the dimensionally reduced model and compare it to the original one. The third chapter is dedicated to the reduced model *per se*: its spectrum, phase structure and other properties. The fourth chapter will address the restoration of the $Z(3)$ symmetry and is followed by conclusions and outlook.

Chapter 1

Reducing the degrees of freedom

1.1 The Model

Pure gauge chromodynamics on the lattice may be formulated in terms of closed loops on the square lattice Λ with link size a . We will denote its extensions in space and in time directions by L_s and L_0 correspondingly. The lattice is periodic in all directions and its length in the time direction equals the inverse temperature

$$L_0 a = 1/T \tag{1.1}$$

On each link of the lattice we put an $SU(3)$ matrix $U(x; \mu)$; it is linked to the gauge fields $A_\mu(x)$ by

$$U(x; \mu) = \exp iA_\mu(x) \tag{1.2}$$

where g_0 is the bare strong coupling constant. The main requirement for the action is the invariance under local gauge transformation generated by $SU(3)$ matrices $G(x)$

$$U(x; \mu) \rightarrow G^\dagger(x)U(x; \mu)G(x + \mu). \tag{1.3}$$

The simplest such action is the Wilson one-plaquette action

$$S(U) = \beta_3 \sum_{x \in \Lambda, \mu < \nu} \left(1 - \frac{1}{3} \text{Re Tr} U_P^{\mu\nu}(x) \right) \tag{1.4}$$

Here

$$\beta_3 = \frac{6}{ag_0^2} \tag{1.5}$$

is the lattice coupling constant. In (2+1) dimensions g_0^2 has a dimension and sets the scale of the model. The coupling β_3 is inversly proportional to the

lattice spacing and thus proportional to the temperature (for constant L_0). The plaquette variable

$$U_P^{\mu\nu}(x) = U(x; \mu)U(x + \mu; \nu)U(x + \nu; \mu)^{-1}U(x; \nu)^{-1} \quad (1.6)$$

represents a loop around one plaquette. It is easy to show that in so-called "naive" continuum limit when we send the link length to zero and expand the U fields around unity one recovers the Yang-Mills action

$$S = \frac{1}{2}Tr \int d^4x F_{\mu\nu} F^{\mu\nu} \quad (1.7)$$

The partition function is

$$Z = \int dU \exp(-S), \quad (1.8)$$

where dU is the invariant Haar measure. The expectation value of any operator is defined thus as

$$\langle O \rangle = \frac{\int dU O(U) \exp(-S)}{\int dU \exp(-S)}. \quad (1.9)$$

The operators which one frequently is interested in, and which will be the major focus of our consideration are the Polyakov loop, which is a trace of the product of the link variables along the time axis

$$L(\vec{x}) = \frac{1}{3}Tr \prod_{i=0}^{L_0-1} U(\vec{x}, ia; \hat{0}), \quad (1.10)$$

and the spatial Wilson loop, which is a trace of the product of the spatial link variables along the closed path. We will consider only rectangular Wilson loops, so for a rectangle $R = [R_1, R_2]$

$$W(R_1, R_2) = \frac{1}{3} \prod_{\vec{x}, l \in R} U(\vec{x}, l) \quad (1.11)$$

In (2+1) dimension this model has a deconfinement phase transition of the second order. The order parameter (on infinite size lattices) is the Polyakov loop. The critical coupling β_c has been determined precisely in [12] and is 14.74(5) for $L_0 = 4$. We will later use this value as the basic unit and express temperature in units of the critical temperature, using for fixed L_0

$$\frac{T}{T_c} = \frac{\beta}{\beta_c} = \frac{\beta}{14.74}. \quad (1.12)$$

Above the critical point there exists a finite string tension and the Debye screening mass is not zero; screening mass vanishes at the critical temperature.

1.2 Naive reduction

In this section we will briefly review so-called “naive” dimensional reduction. It is a rough approximation of the full reduced model, which we will discuss in Chapter 2. In fact for very high temperatures one may integrate out time-related degrees of freedom. Then we are left with (in our case) a two-dimensional lattice Λ_2 with Wilson action

$$S_W^2 = -\beta_2 \sum_{x \in \Lambda_2} \frac{1}{3} \text{Re Tr} U_P \quad (1.13)$$

with the coupling β_2 being L_0 times bigger than the original coupling of $(2+1)D$ model.

$$\beta_2 = L_0 \beta_3 \quad (1.14)$$

This approximation is particularly interesting due to the fact that this model can be analytically solved. The solution comes up to Gross and Witten [39], here we will sketch the main ideas and present the actual calculation of the string tension (we will need this result in Chapter 2) in Appendix 2.

Let us consider an infinite (or with open boundary conditions) $2D$ square lattice as described above. Due to the nature of our $2D$ model we will use symbolics $\hat{1}$ and $\hat{2}$ for directions x and y , leaving $\hat{0}$ for the time direction. For this model the following gauge may be introduced. First, we set an arbitrary gauge matrix in the coordinate system origin and gauge all link variables in $\hat{2}$ direction to one. Then, starting from this line, we set all links in $\hat{1}$ direction to unity (like in the static gauge, although we do not have time-direction now) and have thus:

$$\begin{aligned} U(x, \hat{1}) &= 1, \\ U(0\hat{1} + n\hat{2}, \hat{2}) &= 1 \end{aligned}$$

Now we introduce the following change of variables

$$U(x + \hat{1}, \hat{2}) \equiv W(x)U(x, \hat{2}), \quad (1.15)$$

so that the action factorizes and the statistical sum becomes

$$Z = \int \prod_x dW_x \exp \left[\sum_x \beta \frac{1}{3} \text{Re Tr} W_x \right] = \quad (1.16)$$

$$= (z)^{V/a^2} \quad (1.17)$$

with

$$z = \int dW \exp \left[\beta \frac{1}{3} \operatorname{Re} \operatorname{Tr} W \right] \quad (1.18)$$

being a one-link integral.

With the same argumentation one can get for the spatial Wilson loop with extensions R and T

$$W_L = (w)^{RT} \quad (1.19)$$

with

$$w = \int dW \frac{1}{3} \operatorname{Tr} W \exp \left[\beta \frac{1}{3} \operatorname{Re} \operatorname{Tr} W \right] \quad (1.20)$$

The string tension is then

$$\sigma = -\ln w = -\log \frac{\partial}{\partial \beta} z \quad (1.21)$$

One can immediately notice that w is always smaller than one; thus string tension is positive, and one is in the confined phase for all coupling values. This is the property which all existing dimensionally reduced models have - no deconfinement phase transition. This reduction is useful only as a reference point; it is not possible to define Polyakov loops and the screening masses in this model.

1.3 Classical reduction

The next step in our consideration is so-called classical reduction. The name "classical" refers to it being performed on the level of action, not taking into account the quantum fluctuations. Consider the general (we will do this in continuum, and use different normalisation of the potential to have the coupling constant in front of the integral) action for a pure gauge $SU(3)$ Yang-Mills theory in (2+1)D:

$$S = \frac{1}{2g^2} \int_0^{1/T} dx_0 \int d^2x \sum_{\mu, \nu=0}^2 \operatorname{Tr} F_{\mu\nu} F_{\mu\nu} \quad (1.22)$$

with the field strength tensor being

$$F_{\mu\nu} = \partial_\mu A_\nu - \partial_\nu A_\mu - ig[A_\nu, A_\mu] \quad (1.23)$$

For very high temperature it seems completely legitimate to ignore the time-dependence of the fields

$$\partial_0 A_\nu = 0 \quad (1.24)$$

Now we can rewrite $F_{\mu\nu}$ in the following symbolic way (latin-style indexes go over spatial directions only):

$$\begin{aligned} F_{\mu\nu} &= F_{km} + \partial_k A_0 - ig[A_k, A_0] + \partial_m A_0 - ig[A_m, A_0] \\ &= F_{km} + D_k A_0 + D_m A_0 \end{aligned} \quad (1.25)$$

with the covariant derivative being

$$D_k A_0 = \partial_k A_0 - ig[A_k, A_0] \quad (1.26)$$

The action then takes the form

$$S \simeq \frac{1}{2G^2} \int d^2x \sum_{k,m=1}^2 Tr F_{km} F_{km} + 2 \sum_{k,m=1}^2 (D_k A_0)^2 \quad (1.27)$$

with the new coupling

$$G^2 = g^2 T \quad (1.28)$$

This is the action with the same gauge group in two dimensions, coupled to the scalar field A_0 which transforms under the adjoint representation of the gauge group. All the fields are called static modes because they do not have any dependence on T . The latter is present only in the coupling constant.

However, as we mentioned before, this procedure is classical and ignores the quantum fluctuations in the system. Detailed consideration performed in e.g. [10] shows that the complete decoupling of the non-static modes is not supposed to be happening in this model.

Chapter 2

Dimensional reduction

2.1 Perturbation Theory

Now we will turn to the actual derivation of the reduced model. We are interested in *gauge invariant* operators, such as the Polyakov loop correlations and the spatial Wilson loops, and those may be computed in any gauge. We will therefore choose the following particular static gauge, which can be realized on the periodic lattice by first setting all A_0 to be independent of the imaginary time coordinate x_0

$$A_0(x_0, \vec{x}) = A_0(\vec{x}) \quad (2.1)$$

This automatically makes the Polyakov loops static operators. Remnants of the gauge freedom are eliminated by adding the so-called Landau constraint

$$\sum_{x_0} \sum_{i=1}^2 [A_i(x) - A_i(x - a\hat{i})] = 0 \quad (2.2)$$

Together with (2.1) this condition is called Static Time-Averaged Landau Gauge (STALG) ([31],[30]). Spatial Wilson loops are not static operators in this gauge.

One can split the field in the static and the non-static components, A_i^{static} and A_i^{ns} which are defined by

$$A_i(x) = A_i^{static}(\vec{x}) + A_i^{ns}(x_0, \vec{x}) \quad (2.3)$$

$$\sum_{x_0} A_i^{ns}(x_0, \vec{x}) = 0 \quad (2.4)$$

The non-static modes should be integrated out, leaving only the static components. We will do this in a perturbative fashion and will omit the superscript "static" then.

It is well known that at the high temperature $Z(3)$ symmetry of the Wilson action is broken and the average of the Polyakov loop is not zero and is close to one of the cubic roots of one. One can eliminate this three-fold degeneracy by rotating the phase away and keeping all gauge variables close to one. In this case one can perform a perturbative expansion, using the Taylor series around unity in arbitrary parametrization satisfying (2.2) and (2.1).

We obtained the effective two-dimensional action according to the standard perturbative techniques ([8],[7],[10]). In momentum space the effective action consists of the classically reduced $3D$ action with all fields not depending on the 0^{th} coordinate (static modes only) and the one-point irreducible Feynman graphs with n - external legs and non-static internal lines, which we will denote by $\tilde{\Gamma}_{ns}^{(n)}$. We have for the n -th order

$$\tilde{S}_{eff}^{(n)}(p_1 \dots p_{n-1}) = \tilde{S}_0^{(n)}(p_1 \dots p_{n-1}) - \tilde{\Gamma}_{ns}^{(n)}(p_1 \dots p_{n-1}). \quad (2.5)$$

It may be proven that $\tilde{\Gamma}_{ns}^{(n)}$ are analytic in momenta due to internal lines having no singularities, so we can expand them around zero momentum and keep only the high-temperature contributions.

Let us see which diagrams we need to calculate. We will limit ourselves to the one-loop approximation. For superrenormalizable theory in 3 dimensions

$$g_R^2 \Lambda = \frac{g_0^2}{a} \quad (2.6)$$

where g_R is the renormalized coupling, g_0 - the bare coupling and Λ is the momentum cutoff parameter. Higher order contributions to $\Gamma_{ns,R}^{(n)}$ get higher powers of Λ , thus smaller powers of T . For diagrams each external leg brings in $(g_R^2 \Lambda)^{1/2}$ in the nominator.

The diagrams with three external legs, which would lead to the terms proportional to the $Tr A_0^3$, are not permitted by the time reversal symmetry of the original action. This symmetry is discussed more in detail in chapters 3 and 4.

The terms with four external legs are of the type $\int d^3k/k^4$ and thus UV-finite. The restriction to the non-static modes $k_0 \neq 0$ makes them also IR-finite. Therefore we computed the corresponding diagrams in the continuum, which is simpler and avoids cutoff effects. The Feynman rules were taken from [46]. The direct calculation was compared to the adaptation of the Nadkarni calculation [9] to the $D = 3$ case.

For the term proportional to the square of the "higgs" field we need the $\tilde{\Pi}_{00}^{ns}(0)$, which is the one loop contribution of the non-static modes to vacuum polarization at zero momenta. Two Feynman graphs contribute, both linearly divergent with Λ . We computed them on the lattice (see Appendix 3), which

provides the cut-off of the order of

$$\Lambda \simeq \frac{1}{a} = TL_0 \quad (2.7)$$

at high temperature.

2.2 Action

The resulting action depends thus on the parameters of the original theory L_0 and β_3 (we will set $a = 1$ from now on). We make a change of variables

$$A_0(x) = \phi(x) \sqrt{\frac{6}{L_0 \beta_3}} \quad (2.8)$$

which will be useful later and express S_{eff}^2 as the function of this field and the two-dimensional gauge field U . It consists of the following three parts:

- pure gauge part S_W^2 , which we had already in "naive" reduction

$$S_W^2 = \beta_2 \sum_{x \in \Lambda_2} Tr \left(1 - \frac{1}{3} \text{Re} U(x; \hat{1}) U(x + a\hat{1}; \hat{2}) U(x + a\hat{2}; \hat{1})^{-1} U(x; \hat{2})^{-1} \right) \quad (2.9)$$

$$\beta_2 = L_0 \beta_3 \quad (2.10)$$

- gauge covariant kinetic term, depending both on U and ϕ , obtained by expanding the S_W^3 to the second order in A_0 (we had it already in "classical" reduction)

$$S_{U,\phi} = \sum_x \sum_{i=1,2} Tr (D_i(U) \phi(x)) \quad (2.11)$$

with D_i being covariant derivative

$$D_i(U) \phi(x) = U(x; \hat{i}) \phi(x + a\hat{i}) U(x; \hat{i})^{-1} - \phi(x). \quad (2.12)$$

Now one can easily see the reason for the normalization of the Higgs-field (2.8) - the classical limit of the kinetic term is $Tr (\partial_i \phi)^2$.

- self-interaction term S_ϕ , which we will also call "Higgs potential"

$$S_\phi = h_2 \sum_x Tr\phi^2(x) + h_4 \sum_x (Tr\phi^2(x))^2 \quad (2.13)$$

with the couplings

$$h_2 = -\frac{9}{\pi L_0 \beta_3} \mu, \quad (2.14)$$

$$\mu = \left(\log L_0 + \frac{5}{2} \log 2 - 1 \right), \quad (2.15)$$

$$h_4 = \frac{9}{16\pi\beta_3^2}. \quad (2.16)$$

We note here that the second term in the action contains both terms of the type $(Tr\phi^2(x))^2$ and $Tr\phi^4(x)$ which are related to each other via

$$(Tr\phi^2(x))^2 = 2Tr\phi^4(x) \quad (2.17)$$

in the case of $SU(3)$ group (or, in our case, for the variables which are related to it via multiplication by a constant factor).

The coupling h_4 comes from the diagrams with four external legs, while the quadratic coupling is expressed via

$$h_2 = -\frac{6}{\beta_3} \tilde{\Pi}_{00}^{ns}(0) \quad (2.18)$$

which can be numerically calculated from Eq.(A.52). We used, however, the scaling form of this quantity (2.14), that is its asymptotic value at large L_0 for the reason that we assume (and prove) that we work in the scaling region of the model (see subsection 2.4.2). The details of the derivation can be found in Appendix 3.

Let us now have a closer look at this action. Unlike the quadric coupling h_4 , which is positive and insures boundedness of the partition function at large fields, the quadratic coupling h_2 is negative. The potential thus has a shape typical for the gauge symmetry breaking by Higgs mechanism. Of course, this symmetry breaking is not expected to happen in two dimensions. In fact, the form of this coupling can be seen as the counter-term for the logarithmic ultra-violet divergence of the two-dimensional model, here prescribed in advance by the UV regularization of the original model. The actual infrared behavior of the model is highly non-perturbative.

In the static gauge the Polyakov loop operator is given in 2 and (2+1) dimensions by the same function of the A_0 field. According to our normalization of the ϕ -field it reads

$$L(x) = \frac{1}{3} Tr \exp (i\phi(x)/\sqrt{\tau}) \quad (2.19)$$

with

$$\tau \equiv \frac{\beta_3}{6L_0} = \frac{\beta_2}{6L_0^2} = \frac{T}{g_3^2} \quad (2.20)$$

being a dimensionless temperature.

Along the line of constant physics ($\tau = const$) the operator used to probe dimensional reduction remains unchanged, and it is thus consistent to compare the correlations of the Polyakov loops measured in three dimensions at the same fixed τ value. The continuum limit is $L_0 \rightarrow \infty$, and large distance behavior can be checked within either one of the two models.

Let us now consider the effective action S_{eff}^2 as a function of the dimensionless temperature τ and the parameter of the original lattice L_0 . After setting

$$a^2 g_2^2 = \frac{6}{\beta_2} \quad (2.21)$$

and using the equations above we find the following form for the three dimensionless couplings

$$a^2 g_2^2 = \frac{1}{\tau L_0^2} \quad (2.22)$$

$$h_2 = -\frac{3}{2\pi} \frac{c_0 \log L_0 + c_1}{\tau L_0^2} \quad (2.23)$$

$$h_4 = \frac{1}{64\pi} \frac{1}{\tau L_0^2} \frac{1}{\tau} \quad (2.24)$$

One can easily see that apart from the logarithmic corrections all three couplings scale as $1/L_0^2$ with L_0 . As a function of τ , h_4 is τ -times smaller than the two other ones.

Let us now write down the effective Lagrangian \mathcal{L}_{eff} as a result of the small a expansion of the effective action S_{eff}^2 . We make a substitution $A_i \rightarrow a g_2 A_i$, $\sum_x \rightarrow a^{-2} \int d^2x$ and use T and g_2^2 as the parameters instead of β_3 and L_0 and

take the limit $a \rightarrow 0$ everywhere but in the logarithmic term. We get

$$\mathcal{L}_{eff} = \frac{1}{4} \sum_{c=1}^8 F_{ij}^c F_{ij}^c + Tr [D_i \phi]^2 + \frac{g_2^2}{32\pi} \frac{g_2^2}{T^2} Tr \phi^4 + \mathcal{L}_{CT} \quad (2.25)$$

$$D_i \phi = \partial_i \phi + i g_2 [A_i, \phi] \quad (2.26)$$

$$F_{ij} = \partial_i A_j - \partial_j A_i + i g_2 [A_i, A_j] \quad (2.27)$$

$$\mathcal{L}_{CT} = \frac{3g_2^2}{2\pi} \left[-\log aT + \frac{5}{2} \log 2 - 1 \right] Tr \phi^2. \quad (2.28)$$

This is a two-dimensional $SU(3)$ gauge invariant Lagrangian for the adjoint scalar field ϕ ; it is far from being the most general one. The gauge coupling g_2 has canonical dimension one in energy and sets the scale. The non-kinetic quadratic term is the counterterm, suited to a lattice UV regularization with spacing a . The quadric self-interaction

$$\hat{h}_4 = g_2^2 \frac{g_2^2}{T^2} \quad (2.29)$$

goes to zero as the temperature approaches infinity and presumably plays a marginal role.

It is easy to identify the symmetries of the reduced action. The space inversion symmetry of the original model remains untouched, as well does the rotational symmetry in the space-like plane. The time direction reversal symmetry, as we pointed out above, turns now to the invariance of the action with respect to changing the sign of the higgs fields, so we define

$$R_\tau : \phi \rightarrow -\phi \quad (2.30)$$

2.3 Simulations

To fulfill our aim of direct and detailed comparison, we had to simulate both the three dimensional and the two dimensional models. For the three dimensional part we used the Quadrics QH2 parallel computer of the Bielefeld University. We refer to [28] for the detailed description of this machine. The actual presented data are combined data from C.Legeland and M.Luetgemeyer, which were crosschecked with the data obtained by the program independently written by the author (based on a different simulation design model of the Bielefeld Lattice Group). Both 3D programs use the Cabbibo-Marinari pseudo-heatbath update algorithm, based on updating the $SU(2)$ subgroups of the $SU(3)$ matrix using Kennedy-Pendelton algorithm. No additional technique like smearing was used.

The two-dimensional project was realized on our farm of PCs. It consists of one server and 10 diskless clients, each having AMD K6 processor at 300MHz clock speed. The cluster was gradually upgraded to a set of AMD Athlon processors, first to 600MHz and then to 1200MHz ones, which are (apart from the linear scaling with the clock speed) considerably more effective in floating point operations. Booting of the clients is done via traditional etherboot [61] which resides on the network cards and boots system from the server. The farm runs under Linux operating system from RedHat with appropriately modified kernel. It provides Message Passing Interface (MPI) services via Los-Alamos MPI Daemon (LAMMPS) from the University of Notre-Dame [62].

The two-dimensional program (written in collaboration with P.Bialas using parts of the standard Bielefeld C++ Monte-Carlo code) consists of two main parts - master and slave.

Master part:

- runs on server
- reads and parses the configuration file
- gives an appropriate set of parameters to all slave nodes. Parameters can be either different for exploring a certain area in coupling constants or the same for accumulating statistics.

Slave part:

- runs on clients
- gets the parameters
- does the actual simulation
- outputs the results

The program is realized in an object-oriented way using classes *lattice* (SU(3) group) and *higgs* (SU(3) algebra). Measurements are done via classes *basic_observables* (all local observables), *corr_observables* (all correlations) and *swl_observables* (non-local observables). All measurement classes are inherited from the class *observable* which does pre- and post-processing as well as output.

For updating gauge fields we used the same algorithm as above, but after *each subgroup* update the resulting matrix was subjected to the Metropolis

question on the hopping term. This approach results in an acceptance ratio of about 95%.

Alternatively we tried the multi-hit Metropolis algorithm. An update of a single link variable was attempted several times (typically eight) before attempting to update the next variable. The trial matrices were generated according to

$$U \rightarrow \exp(i\delta A)U$$

where δA was a Hermitian matrix generated from the distribution $\exp(-\epsilon \text{Tr} A^2)$. The parameter ϵ was tuned to obtain the acceptance ratio close to 50%. Because generation of the trial matrices is expensive in CPU time (for it requires matrix exponentiation), we stored the values in the table for later use (that is we store both the matrix and its conjugate to ensure the detailed balance). This table was updated every five sweeps. The autocorrelation times were comparable to heat-bath but the CPU time required to perform the metropolis update was approximately two times bigger.

The scalar fields were updated using multi-hit metropolis. At every point we tried as before typically eight updates. New scalar fields were obtained from

$$A \rightarrow A + \delta A$$

where δA was generated the same way as above, using the same desired acceptance rate. One sweep over lattice consisted of one update of the gauge fields followed by one update of the scalar fields.

Operators we measured were:

- the "control" variables $\text{tr} A^2$, $\text{tr} A^3$ and $\text{tr} A^4$
- plaquette variables averages
- Polyakov loops (defined by (1.10) in 3D and (2.19) in 2D) and their on-axis correlations

$$L(r) = \frac{1}{2} \langle L(x)L(x+r) + L(x+r)L(x) \rangle - \langle L(x) \rangle^2 \quad (2.31)$$

where the averaging is performed over lattice and computer time. When necessary we will use indexes $D = 2 + 1$ or 2 specifying the dimension considered.

- Spatial Wilson loops $W(r_1, r_2)$ (defined in the same way both in 2D and 3D)

We used the following tests to test the program:

- **Gauge Sector:** remove interaction (kinetic) term in the update routine. Then the model is reduced to the pure gauge theory with action (1.13) and can be compared to the analytic solution.
- **Higgs Sector:** set the β_3 and the quadric coupling to zero. The model is reduced to the free-field model for the scalar fields which can be exactly solved.
- **Polyakov loop Correlations:** same as in latter case, may be expanded and calculated in the small field limit

The analytic solution and results for the two last test are presented in the Appendices 4 and 5.

All runs in the main simulation of the two dimensional model were performed on 32×32 lattices with the parameter L_0 set to 4. The dynamics of the gauge and Higgs sector turned out to be quite different. The integrated autocorrelation time for the plaquette was typically of the order of one while for the Higgs related local variables (e.g. $tr A^2$) it varied between 100 and 400 sweeps when β_3 varied between 21.0 and 346.0. For each β value we collected typically one million sweeps.

2.4 Polyakov loop correlations and Masses

2.4.1 Comparison with the original model

The Polyakov loops correlations defined as in Eq.(2.31) were measured every ten sweeps. While due to the large autocorrelation times this was in a sense an "oversampling" - it was not too costly in CPU time. The measurements were blocked by 50 and written out. Afterwards the data were analyzed using the double jack-knife method with typically 25 blocks. First, the jack-knife procedure was used in a standard way to get the values of the $L(r)$ and the error estimates. Then these were used to obtain the fit (see below) parameters and the errors (which were uniform for all blocks of the second jack-knife) using the second jack-knife. For checking consistency we also tried a different number of blocks, and the errors, as expected, did not show any significant dependence on the number of blocks in this region.

There are two possible statements of the dimensional reduction about the Polyakov loops

- **Weak:** the lowest state coupled to $L(x)$ is the same in both dimensions, so that the two functions must have the *same shape* in r at large r

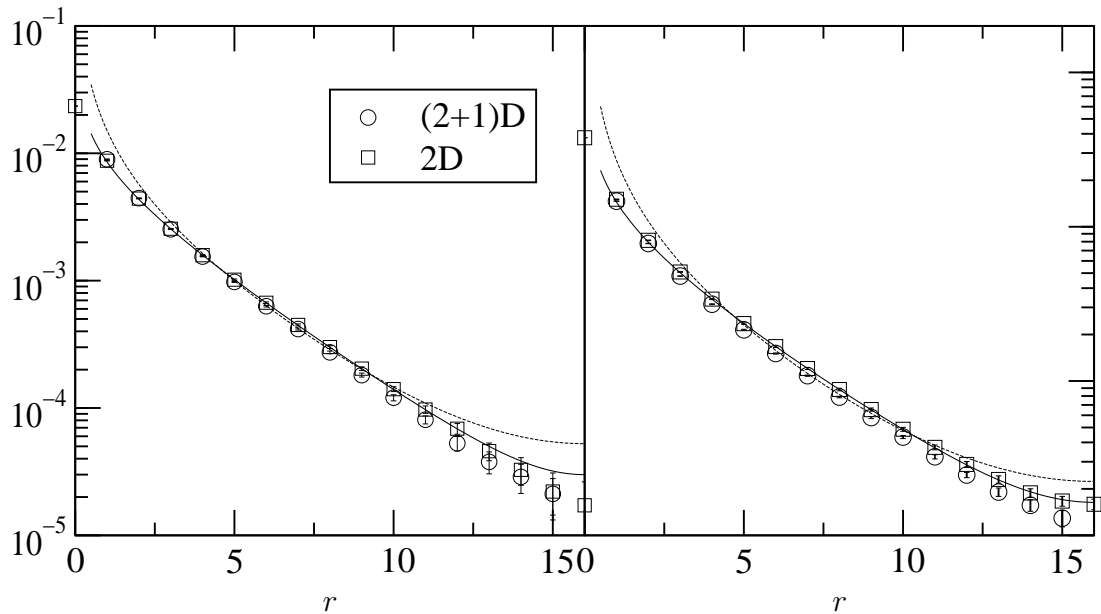


Figure 2.1: Polyakov loop correlations $L_D(r)$, $D = 2 + 1$ (circles) and 2 (squares), for β_3 equal to 29 (left) and 84 (right). Distance r is given in lattice units. In both cases $L_s = 32$ and $L_0 = 4$. The 2D data were produced using h_2 from Eq.(2.14). The continuous and the dashed lines result respectively from fitting formulae (2.34) and (2.33) to the 2D data.

- Strong: to the extent that the weight associated with S_{eff}^2 is a good approximation to the integral over the non-static field of the $(2 + 1)D$ field (in the small p/T regime at least) the averages with the respect to the two weights of a static operator, such as $L(r)$, are equal at large r

We will show that the latter situation is approached at sufficiently high temperature. Using $L_0 = 4$ fixed, we investigate the temperature dependence of the correlations by varying β_3 in the range $[21, 173]$. High temperature means β_3 sufficiently larger than the transition point in $(2 + 1)D$. These β_3 values correspond roughly to temperatures in the range $T/T_c \in [1.43, 11.73]$

On the Fig.2.1 the correlations $L_{2+1}(r)$ and $L_2(r)$ for $\beta_3 = 29.0$ and 84.0 are presented. We see that the two correlations are extremely close to each other: not only they have the same *shape* at large r , which is the primary prediction of dimensional reduction, but also nearly the same *normalization*. As announced, this finding favours dimensional reduction in the strong sense.

In addition, we notice that this agreement between the two ways of computing the Polyakov loop correlation extends down to fairly small values of r . Since the normalization is set by $|\langle L(\vec{x}) \rangle|^2$, it shows that, although it is lo-

cal, the Polyakov operator is not very sensitive to the short wave length terms omitted in the effective action. In Table 2.1 we present the results for $\langle L_2 \rangle$ and $\langle L_{2+1} \rangle$ to demonstrate this property. Relatively to their distance to one (their common value at $\beta_3 = \infty$), their difference, already $\sim 6\%$ at $\beta_3=21$ ($T/T_c = 1.43$), decreases to only about 0.6% at $\beta_3 = 173$ ($T/T_c = 11.73$).

β_3	$ \langle L_2 \rangle $	$ \langle L_{2+1} \rangle $
21.0	0.56002 (62)	0.53467 (16)
29.0	0.67007 (25)	0.66120 (13)
42.0	0.76397 (20)	0.76130 (12)
84.0	0.87392 (11)	0.87435 (6)
173.0	0.93494 (13)	0.93530 (11)

Table 2.1: The average Polyakov loop as a function of β_3 in $(2 + 1)$ D and 2D.

In Fig.2.2, we illustrate more in details, for the β_3 values not reported on in Fig.2.1, how well the $2D$ and $(2 + 1)D$ correlations compare. Their ratio L_{2+1}/L_2 is plotted against the distance r in lattice units. These data definitely support the statement that L_{2+1}/L_2 remains quite flat and close to one for all distances and temperatures. Recalling that the lowest T value is only ~ 1.5 times T_c , and that the correlation functions decrease in r by about three orders of magnitude, we conclude that the effective local 2D action reproduces the $(2 + 1)D$ Polyakov loop correlations with a remarkable accuracy, soon above the transition and down to distances even shorter than $1/T$.

2.4.2 Scaling test

As for every lattice calculation, the question arises if the lattice size is sufficient for the study, or finite size effects influence the measurements. This is normally checked by running the same simulation on the larger lattices and comparing results. The parameters of the bigger lattice are defined as follows. Given the temperature, the continuum limit is approached by taking

$$\tau = \frac{\beta_3}{L_0} = \frac{T}{g_3^2} \quad \text{fixed} \quad L_0 = \frac{1}{aT} \quad \text{large} \quad (2.32)$$

Scaling region is then defined as the region where physics of the model at fixed τ does not depend on L_0 , if L_0 is large enough. To check if we are in

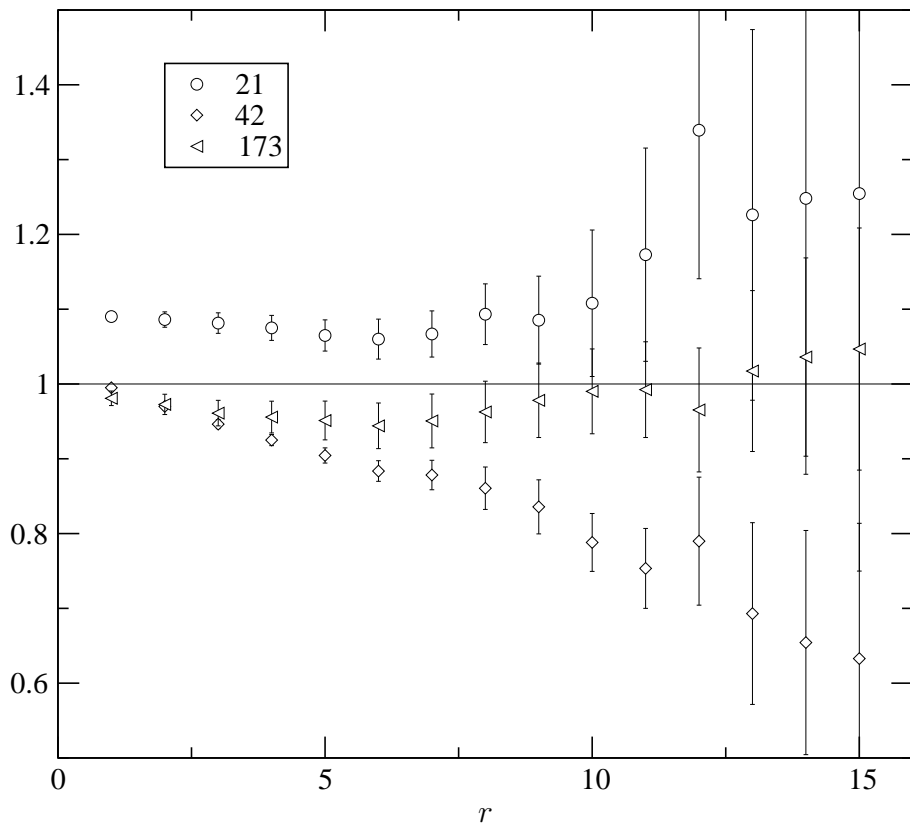


Figure 2.2: Ratios $L_{2+1}(r)/L_2(r)$ of Polyakov loop correlations as functions of the lattice distance r for $T/T_c = 1.4, 2.8, 11.7$ ($\beta_3 = 21, 42, 173$).

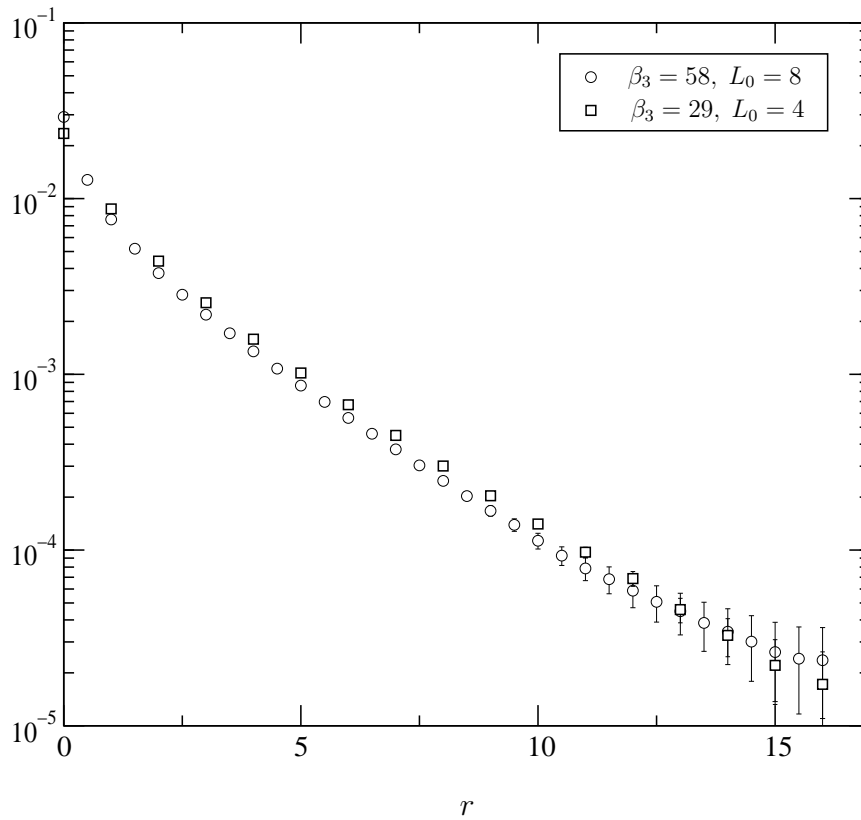


Figure 2.3: Comparison of the Polyakov loop correlations in the 2D model for the two sets of parameters corresponding to $T/T_c = 1.97$ $[\beta_3, L_0, L_s] = [29, 4, 32]$ and $[58, 8, 64]$ i.e. for constant τ (2.20). The values of r for $L_0 = 8$ (circles) are scaled down by a factor two in order to maintain the same physical scale.

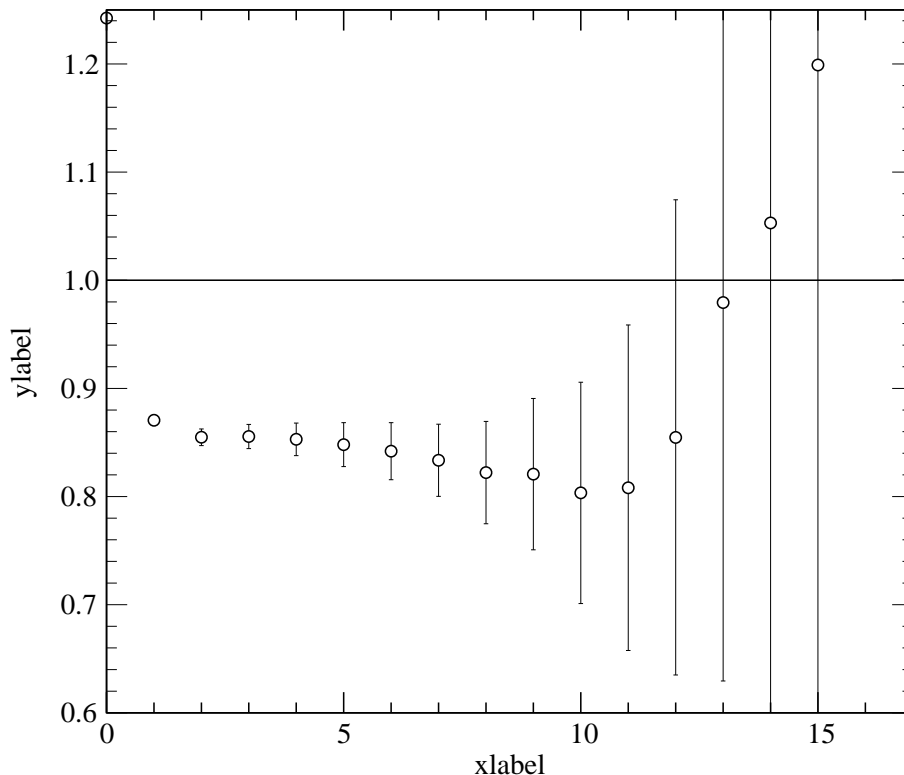


Figure 2.4: The ratio between the two Polyakov loop correlation functions presented in figure 2.3.

this region, we compared the Polyakov loop correlations in $2D$ for two sets of the lattice parameters, namely $[\beta_3, L_0, L_s] = [29, 4, 32]$ and $[58, 8, 64]$. Given T , doubling L_0 means dividing the lattice spacing a by two, so that the *physical* spatial size aL_s of the lattice is unchanged. The resulting correlations are presented in Fig.2.3 showing a very similar shape as a function of the physical distance. It is again instructive to consider their ratio, found to be quite flat at all distances (Fig.2.4): within errors, there is no sizable deviation from scaling.

The other observation is that this constant ratio is not one. And it should not be because it is given by the corresponding values of $|\langle L(\vec{x}) \rangle|^2$. They are not physical quantities due to explicit (logarithmic) dependence of the $2D$ effective Lagrangian on a via its counterterm Eq.(2.28).

Hence scaling is verified in the range of interest. It justifies keeping $L_0 = 4$, which is less expensive in computer time and allowed us to use the existing data of [28] in $(2 + 1)D$.

2.4.3 Screening Lengths

The fast decay of the correlation functions with r is consistent with the existence of a finite spatial correlation length, ξ_S , associated with the quantum numbers of the Polyakov loop operator, a color singlet scalar. A mass can be defined as usual by $M_S = \xi_S^{-1}$.

For the (3+1) dimensional model D'Hoker advocated the scenario (based on perturbation theory) that the screening mass M_S is $2M_E$, twice the so-called electric screening mass, because the lowest “state” coupled to the loop is a two electric gluon state [27]. In this case the $L(r)$ correlation is expected to be proportional at large r to the square of the correlation function for a one particle state of mass M_E :

$$L_D^{(2m_E)}(r) \simeq c' \left(\frac{1}{[m_E r]^{1/2}} e^{-m_E r} + \frac{1}{[m_E(L_s - r)]^{1/2}} e^{-m_E(L_s - r)} \right)^2. \quad (2.33)$$

In the present case, however, the infrared sector is more complicated and perturbation theory is doubtful. One of the options is that there exists in the Polyakov loop channel an *independent* screening mass M_S , associated with a true excitation of the $2D$ system. In this case we parametrize the data according to

$$L_D^{(m_S)}(r) \simeq c \left(\frac{1}{[m_S r]^{1/2}} e^{-m_S r} + \frac{1}{[m_S(L_s - r)]^{1/2}} e^{-m_S(L_s - r)} \right). \quad (2.34)$$

The second term in both cases arises from the finite size of the lattice and its form is determined by the periodicity. It actually does improve fitting process significantly. The m symbols denote masses in lattice units, i.e. $m \equiv aM$. These parametrizations respect the lattice symmetry $r \rightarrow L_s - r$. Since we have no direct access to m_E , the two expressions above differ in shape through the prefactors, $r^{-1/2}$ and r^{-1} respectively. We checked that for $r > 1$ lattice artefacts are negligible in the mass range considered. This was achieved by comparing Eq.(2.34) to the lattice propagator

$$L_{Latt}(m_S, r) = \frac{1}{L_s^2} \sum_{p_1, p_2} \cos(p_1 r) \tilde{L}_{Latt}(m_S, \vec{p}), \quad (2.35)$$

$$\tilde{L}_{Latt}^{-1}(m_S, \vec{p}) = \hat{p}^2 + 4 \sinh(m_S^2/4). \quad (2.36)$$

We carefully analyzed our numerical data, and *we find that the ansatz* (2.34) *is by far the best one*, giving a good fit of the data down to small r values. For an illustration, the continuous curves of Fig.2.1 are fits of the form (2.34) to $L_2(r)$, $r \geq r_{min}$, with $r_{min} = 4$, and changing r_{min} from 3 to 6 does not change

the resulting m_S within errors. At the shorter distances a noticeable deviation exists, which can be either due to the presence of the more massive contribution or just be an artefact of the lattice UV regularization. It is anyway too small to be reliably analyzed. On the contrary fits to the same data of the form Eq.(2.33) lead in Fig.2.1 to the dashed curves, which are clearly not acceptable. The results of systematic fits of expression (2.34) to all available correlations $L_2(r)$ and $L_{(2+1)}(r)$ are presented in Fig.2.5. We define the corresponding dimensionless quantities

$$M_S/(g_3\sqrt{T}) \equiv m_S\sqrt{L_0\beta_3/6} \quad (2.37)$$

$$g_3^2/T \equiv 6L_0/\beta_3 \quad (2.38)$$

and plot them one versus the other.

It is also interesting to check to which extent the calculated coefficients are important for the simulations and if they have only minor effect. Thus we also plot the masses resulting from a few simulations made with the classically reduced effective action ($h_2 = h_4 = 0$). They are far away from the former, showing the important effect of taking into account the non-static degrees of freedom. One may also want to check if the simulation which uses the so-called scaling form (2.14) of h_2 differs much from the simulation with the value obtained numerically from Eqs. (2.18, A.52). The results are similar, especially at high temperature, but anyway distinguishable within our statistical accuracy. This shows a great sensitivity of the static properties to the quadratic counterterm (2.28), an interesting feature *per se*.

The scaling properties observed in the previous subsection reflect themselves of course in the mass values. For the two cases compared there, we find $M_S a = 0.331(6)$ and $0.169(3)$: the lattice spacing is reduced exactly by two within errors. Of course the fact that dimensional reduction works well for masses directly follows from its success for correlations. We preferred to illustrate it first on directly measured quantities, as done in Fig.(2.3). This comparison does not depend on any interpretation of the nature of the observed screening lengths.

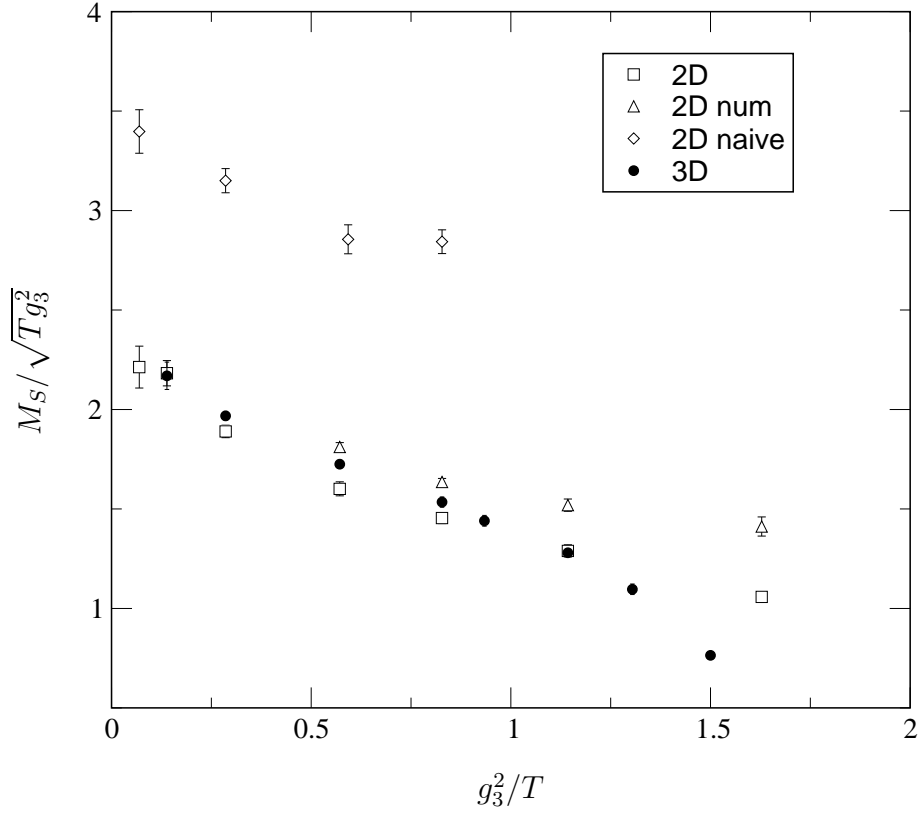


Figure 2.5: Physical screening masses M_S in units of $g_3\sqrt{T}$ versus g_3^2/T , in $(2+1)D$ (black points) and $2D$ (squares). Also shown are the masses obtained with the numerical value of h_2 from Eq.(2.18) (triangles) instead of its asymptotic expression (2.14), and with the classically reduced (labeled naive) action: no Higgs potential, $h_2 = h_4 = 0$. Masses of the original model vanish at critical point, while in reduced one they do not

2.5 Spatial Wilson loop

The spatial Wilson loops are measured on a lattice via

$$\tilde{W}(R, R', x, y, m) = \prod_{i=0}^{R-1} U(x+i, y, \hat{0})_m \prod_{j=0}^{R'-1} U(x+R, y+j, \hat{1})_m \times \quad (2.39)$$

$$\times \prod_{i=R-1}^0 U^\dagger(x+i, y+R', \hat{0})_m \prod_{j=R'-1}^0 U^\dagger(x, y+j, \hat{1})_m \quad (2.40)$$

$$W(R, R') = \frac{1}{N_m} \sum_{m=1}^{N_m} \frac{1}{V} \sum_{x,y=0}^{L_s-1} \tilde{W}(R, R') \quad (2.41)$$

where N_m is the number of measurements, and index m refers to the particular measurement.

In our simulations the Wilson loops were measured every ten sweeps and blocked by 50. Integral autocorrelation time for the measurements of 14×14 Wilson loops was, in the worst case, of the order of one and was negligible in the majority of cases. The measurement routine is quite expensive and consumed almost half of the CPU time.

In order to extract the string tension, local potentials were first extracted from the ratios :

$$V(R, R') = \log \frac{\langle W(R, R') \rangle}{\langle W(R, R'+1) \rangle}. \quad (2.42)$$

By definition, the potential is

$$V(R) = \lim_{R' \rightarrow \infty} V(R, R'). \quad (2.43)$$

For each given R , $V(R, R')$ was found to decay exponentially to a constant in R' . In practice, the constant regime is reached within errors above $R' = 3$ and the potential was fitted in the range $R' \in [4, 12]$. The string tension σ was then obtained from the ansatz

$$V(R) = V_0 + \sigma R. \quad (2.44)$$

The errors on the string tension were calculated using the triple jack-knife method as follows:

1. split the data into N blocks
2. omitting one block at time, produce N sets, each consisting of $(N - 1)$ blocks

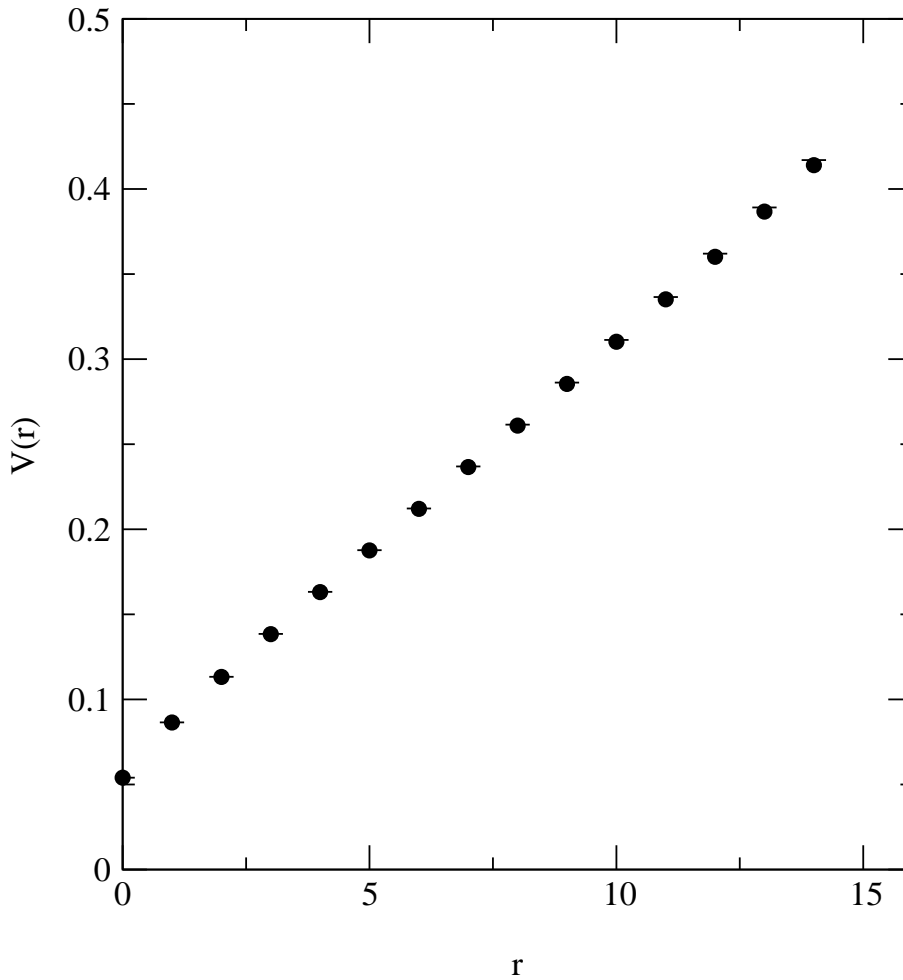


Figure 2.6: Potential extracted from the spatial Wilson loops, $\beta_3 = 42$

3. in each of the sets repeat this procedure, so that we get $N \times (N - 1)$ sets each consisting of $(N - 2)$ blocks
4. use these in traditional jack-knife way to obtain $N \times (N - 1)$ sets of $V(R, R')$ with errors
5. repeat it to obtain N copies of the $V(R)$ with errors (which we need to do the weighted fitting)
6. fit to the formula (2.44) get string tension and errors

A typical form of the potential is presented in Fig.2.6. A fit using the linear potential (2.44) is sufficient to obtain a stable value of σ within errors.

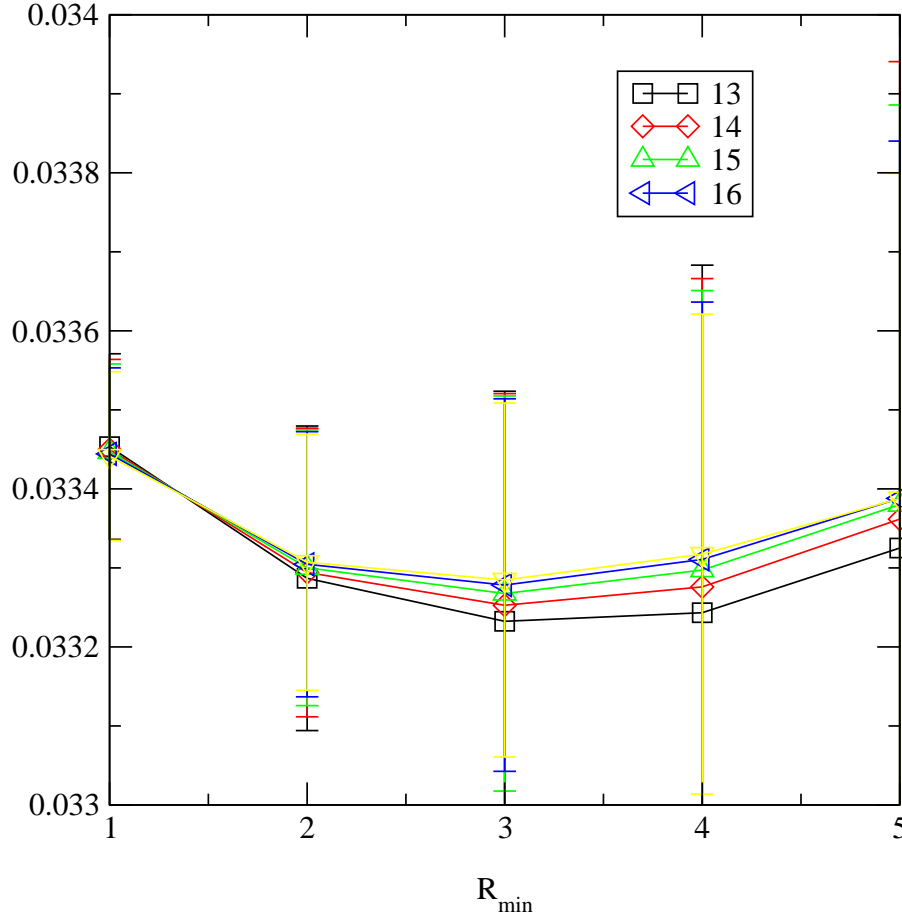


Figure 2.7: We plotted string tension for 4 different upper cutoff values against lower cutoff value

To prove that, we produced for every β_3 a fit from R_{min} to R_{max} . The R_{max} values, depending upon the value of β_3 , varied from 10 to 14, the R_{min} varied from 1 to 4. To judge about stability of the fit we plotted the resulting value of σ with errors as the function of R_{min}, R_{max} . As it may be seen from Fig.2.7 the fit is indeed stable. This is in good agreement with fluctuating flux tube model [36] - the Luescher $1/R$ term is not expected to be present above the phase transition.

The χ^2 value in the 3D case was of the order of one and about ten times less in the 2D case, likely due to the large correlation between points.

For the dimensionally reduced treatment the case of the spatial Wilson loop W in 3D is more difficult than the Polyakov loop correlations. It is not a static operator, and thus by no means is predicted to be reproduced well in the

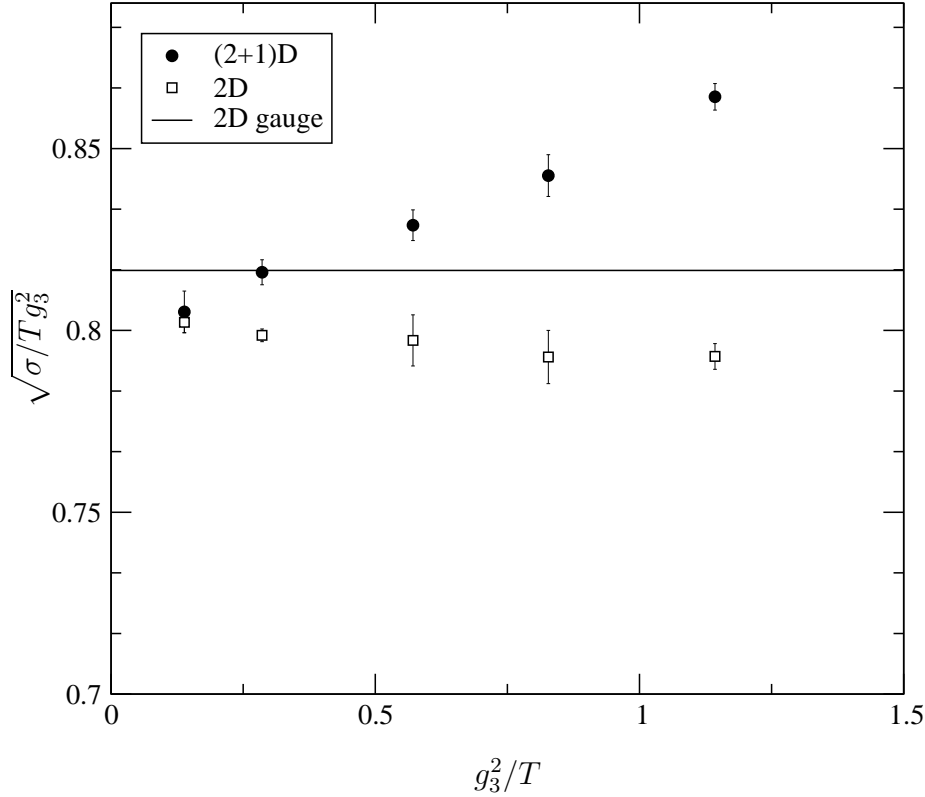


Figure 2.8: The square root of the physical string tension in units of $g_3\sqrt{T}$ as a function of g_3^2/T in (2+1)D (filled circles) and 2D (squares). The line denotes the scaling limit $\sqrt{2/3}$ in 2D pure gauge theory (1.21).

dimensionally reduced model in the high temperature region. However, there are the following considerations:

- i) a non-zero spatial string tension σ_{2+1} is known to exist [28] above the deconfinement temperature
- ii) the pure gauge 2D theory is confining and produces a finite string tension σ_2^0 [39]
- iii) in two dimensions we expect confinement and thus a finite string tension σ_2^ϕ to survive when the Higgs field ϕ is turned on.

It is thus interesting to compare these three quantities as a function of the temperature of the $(2+1)D$ model. For this comparison we take $a^2\sigma_{2+1}$ and

$a^2\sigma_2^\phi$ from the analysis of W data provided by [28] and by our simulation, whereas $a^2\sigma_2^0$ is computed analytically in Appendix 2:

$$a^2\sigma_2^0 = \frac{4}{\beta_2} + \frac{7}{\beta_2^2} + \mathcal{O}(\beta_2^{-3}).$$

The next terms in this expansion are easy to derive using the computer algebra system. However, they are not required for our purpose. This expression can be equivalently rewritten

$$\frac{\sigma_2^0}{g_3^2 T} = \frac{2}{3} + \frac{7}{36} \frac{g_3^2}{T} (aT)^2 + \mathcal{O} \left[\left(\frac{g_3^2}{T} \right)^2 (aT)^4 \right],$$

showing that up to scaling violations of order

$$(aT)^2 = \frac{1}{L_0^2} \tag{2.45}$$

σ_2^0 scales as $2g_3^2 T/3$ at finite T . The quantities reported in Fig.2.8 versus g_3^2/T are the values of $\sqrt{\sigma}$ in units of $g_3\sqrt{T}$, which we thus compare to $\sqrt{2/3}$. The numerical values of $\sigma_2^\phi/(g_3^2 T)$ and $\sigma_{2+1}/(g_3^2 T)$ were obtained from the simulations for $L_0 = 4$.

All three string tensions are quite close to each other; they differ by at most 10% within our temperature range. From the two-dimensional point of view, we see that introducing the ϕ field modifies the picture quite weakly: no sizable g_3^2/T dependence around a value close to $\sqrt{2/3}$. The behavior for σ_{2+1} is different, with a sizable slope in g_3^2/T . The difference observed between σ_{2+1} and σ_2^ϕ may be understood as a consequence of W not being a static operator: the average of its non-static modes with the $(2+1)D$ weight are missing in its calculation with the effective action. However, scaling violations may also contribute differently to these two σ 's, so that definite conclusions require complementary simulations.

Another possible reason for this disagreement are the heavy space correlations in the Wilson loops measurements, which may lead to systematic errors for the σ measurements. Our data, presented in Fig.2.8, do not lead to the definite conclusion whether or not the infinite T limit of the string tension in the two- and three-dimensional models is the same, and if it is equal exactly to $2/3$.

Chapter 3

Reduced Model Per Se

3.1 Phase structure of the model

As we have seen in the previous chapter, the reduced model reproduces the $(2 + 1)D$ model very well; it is interesting thus to study the properties of the reduced model as such. As we pointed out in Chapter 2, the wanted deconfinement phase transition is absent in this model; one can see it either from the fact that screening masses do not vanish, or via direct test. The reason for that is the explicitly broken $Z(3)$ symmetry in the perturbative approach. One of the remaining symmetries is the R_τ (see 2.30) - the imaginary time reversal symmetry of the original model. As it was pointed out in the studies of the $(3+1)D$ case, there exist two phases, symmetric and broken with respect to this symmetry. The same scenario happens also in our model. The test runs on the small lattices have shown the possibility of the very different dynamics of the system. Indeed, we were able to see a strong first order phase transition happening. The order parameter for this transition is

$$O_1 = \langle tr A^3 \rangle \tag{3.1}$$

It is equal to zero in all the simulations discussed previously and is different from zero in the broken phase.

We performed extensive simulations for lattice sizes 8×8 and 6×6 with parameter $L_0 = 4$. To see how the transition point moves with scaling we also simulated on 8×8 , 10×10 and 12×12 lattices with $L_0 = 8$. Couplings β_2 and h_4 were fixed at three-dimensional values corresponding to $\beta_3 = 29$ ($\beta_2 = 116$, $h_4 = 0.954930$) and $\beta_3 = 58$ ($\beta_2 = 464$, $h_4 = 3.819718$) respectively. The operators of interest this time were $Tr A^2$ and $Tr A^3$. To map the transition point we performed a large number of measurements, which varied from 3.000.000 to 30.000.000 depending upon coupling. The typical autocorrelation time was of the order of several thousands due to closeness to the phase transition.

We used the histogram technique to find out the position of the phase transition. Unlike in the previous chapter, the data were not blocked to increase the statistics for histogramming. Typical histograms for TrA^2 are presented on Fig.3.1 and Fig.3.2 for $L_0=4$ and 8 respectively. They have a clear two-peak structure, which is the traditional picture for the phase transition of the first order. Behavior of the system was significantly different in these cases: for $L_0 = 4$ already at 6×6 lattice a very sharp two-peak structure was present, and two phases are separated clearly. For $L_0 = 8$ the transition is much softer, the relative height of the peaks is smaller compared to the dip. This is compatible with the fact that we decreased the lattice spacing twice when increasing L_0 .

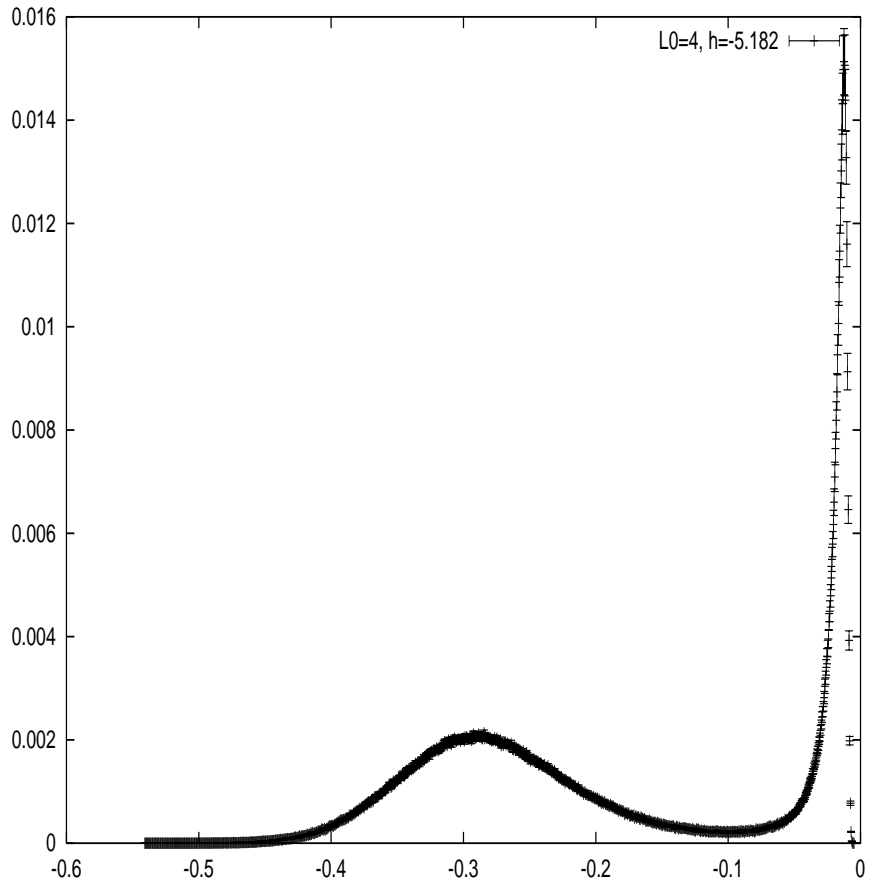


Figure 3.1: Histogram, TrA^2 , 6×6 lattice, $L_0 = 4$

A typical histogram for O_1 is presented on Fig.3.3 - a clear three-peak structure is present; the scaling behavior also turned out to be similar. This histogram shows that in fact there are not two but three different phases,

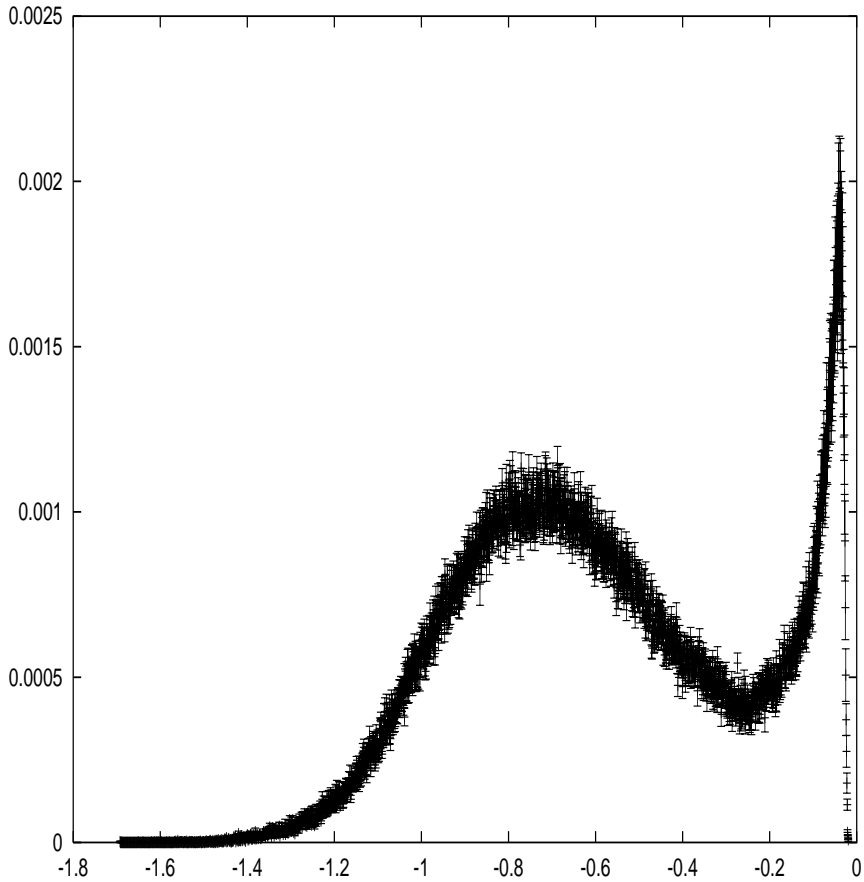


Figure 3.2: Histogram, $Tr A^2$, 8×8 lattice, $L_0 = 8$

the symmetric one and two broken phases with positive and negative value of the order parameter. For the data analysis we used the Ferrenberg-Swendsen multiple histogram reweighting algorithm. It allows to use the data from several histograms, effectively accumulating statistics for a more precise determination of the critical point. Details of the algorithm may be found in [47]. The single histogram reweighting method was used for the cross-checking.

There are several criteria which one may use in case of the first order phase transition, among them the equal weights criteria and the susceptibility criteria. To employ the equal weights criteria we need to take into account that there are three phases. Thus the criteria should be formulated as such that broken phases weight is $2/3$. After scanning the h_2 space, we spotted the approximate point where transition happens and performed about a dozen of long runs in that area. Then we used the Ferrenberg-Swendsen reweighting to produce

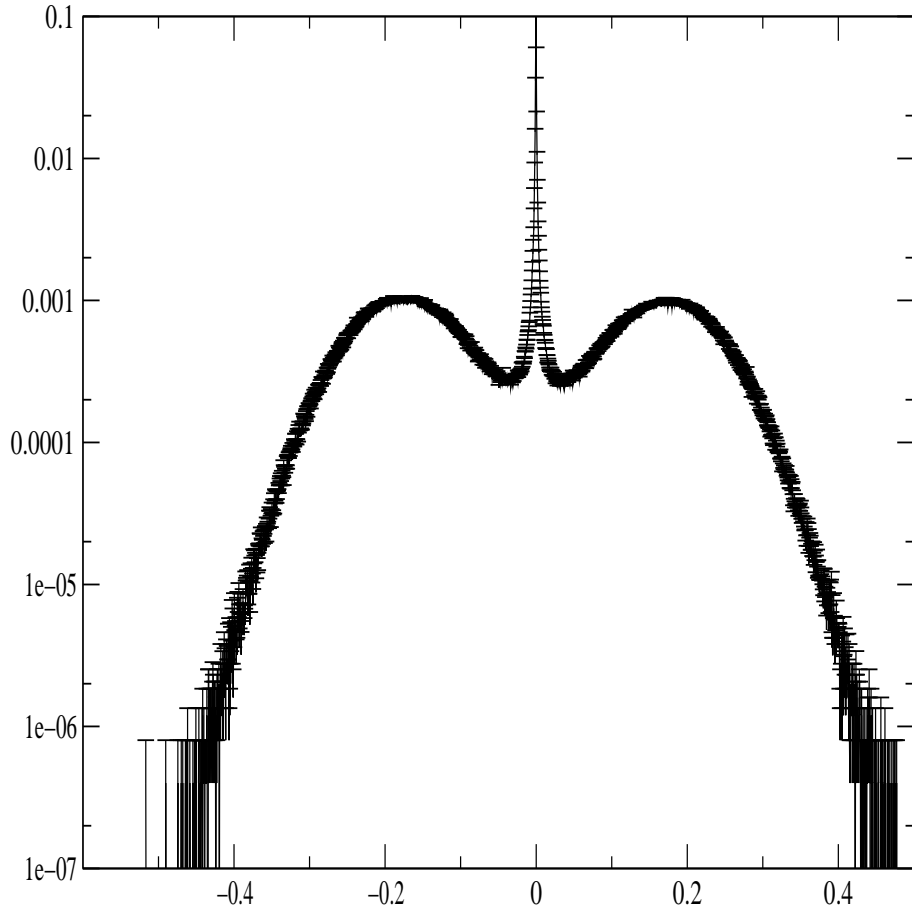


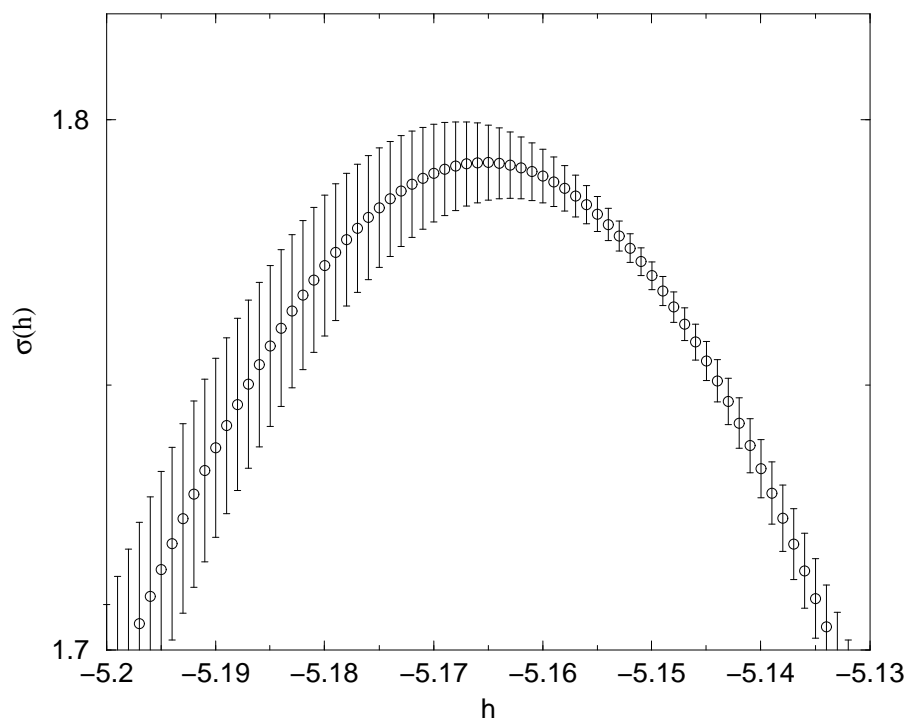
Figure 3.3: Histogram, $Tr A^3$, 8×8 lattice, $L_0 = 4$

the table of the pairs (h_2, W_b) where W_b is the weight of the broken phase (i.e. number of measured values which are on the left side of the minima, divided by the overall number of measurements) with a very small step in h_2 . Afterwards the h_2 corresponding to the closest to $2/3$ value of W_b was selected to be an estimator for the critical point. This estimator was used in jack-knife like treatment to obtain the errors on the critical value of h_2 .

A typical picture for the susceptibility is presented on Fig.3.4 where susceptibility is plotted versus h_2 for $L_0 = 4$. To estimate the $h_{critical}$, we find the absolute maximum for every jack-knife bin, ignoring the actual errors on susceptibility. As it can be seen from table 3.1 below, the susceptibility maximum criteria estimate gets closer to the equal weights criteria one when increasing volume and, moreover, coincides within errors for the bigger value of the parameter L_0 .

Susceptibility maximum criteria

6x6 lattice



	6×6	8×8	∞	$3D$	
equal weights	-5.186(2)	-5.225(4)	-5.275(12)	-6.071	
susceptibility	-5.165(3)	-5.208(4)	-5.263(13)	-6.071	
	8×8	10×10	12×12	∞	$3D$
equal weights	-7.28(2)	-7.33(2)	-7.37(2)	-7.45(9)	-8.06
susceptibility	-7.28(2)	-7.34(2)	-7.39(4)	-7.44(11)	-8.06

Table 3.1: Critical couplings for $L_0 = 4$ and $L_0 = 8$

We also provide in the table the reduced values (labeled 3D) and two extrapolated values, an “infinite volume” value and the 32×32 value, which we need for making the conclusion about where we are on the actual lattice we work on. The scaling behavior of the following type was assumed

$$h_V = h_{\text{inf}} + \frac{C_1}{V} + O\left(\frac{1}{V^2}\right) \quad (3.2)$$

To check the validity of this ansatz we compared the predicted from the two points value for the third point with the actual value, and they agree within errors.

The phase diagram is sketched on Fig.3.5, the dotted line is there to guide the eye. The reduced values are obviously in the broken phase, and situation does not get any better with increasing L_0 . The Polyakov loops and the string tension are not reproduced by the simulations in that phase. However, due to it being a very strong first order phase transition - it never (on a scale of several gigaflops-monthes) happens on the 32×32 lattice which we used in the previous chapter. Starting from a weak field configuration, we are in the symmetric phase and always stay in it.

One could perform here a more detailed analysis following Ref. [13] as done in the determination of the critical exponents and transition temperature in [12] along with the study of the larger lattices. Latter would require some advanced simulation method (e.g. multi-canonical simulations). However, as long as the transition is of a strong first order we conclude that for the small values of L_0 our lattices are big enough to make a statement that the reduced values are in the broken phase.

3.2 The spectrum of the model

In this section we will study the lowest states of the spectrum of the reduced model *per se*. We restrict ourselves to the operators directly related to the

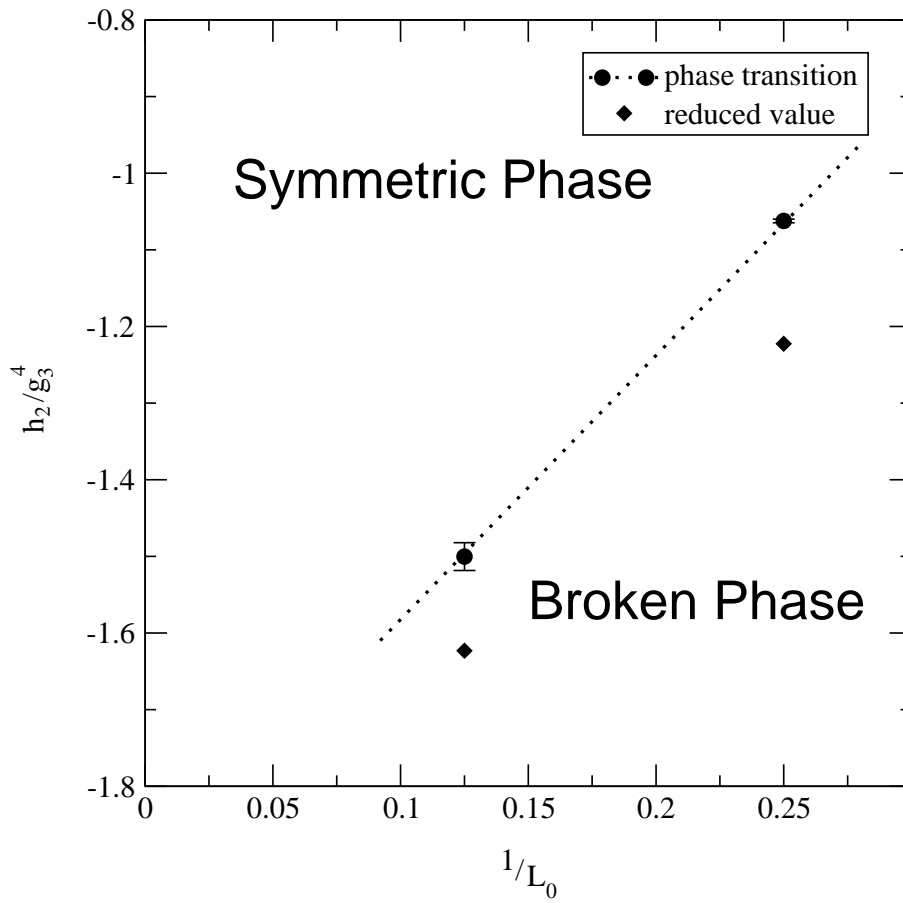


Figure 3.5: Phase Diagram of the Model

static operator $L(x)$ because only they are directly relevant for the $(2+1)D$ system.

Let us now expand the $L(x)$ in powers of $A(x)$ and study the operators $A^n(x)$ and connected correlations of their traces. We define

$$A_n(x) \equiv \text{Tr} A^n(x), \quad (3.3)$$

$$A_{n,m}(x) \equiv \langle A_n(x) A_m(0) \rangle - \langle A_n \rangle \langle A_m \rangle. \quad (3.4)$$

$$A_n \equiv \langle A_n(x) \rangle \quad (3.5)$$

Any operator $A_n(x)$ is gauge invariant, even or odd under the R_τ -symmetry of the $2D$ action for n even or odd respectively. We will continue working in the unbroken R_τ phase only, where $A_{2p+1} = 0$.

Using the same action as in Chapter 2 we have performed a numerical simulation of the two dimensional model for lattice size $L_S = 32$ till the end of the chapter. The β_3 values are 29, 42, 84 and 173, while $L_0 = 4$. They correspond to the values of T/T_c equal approximately to 1.97, 2.85, 5.70 and 11.73 respectively. We were able to extract information from the operators and correlations corresponding to $n = 2$ to 5. The cases $n = 2$ and 3 for the $3D$ reduced model were investigated in [20].

Here we will present our results for the $A_{n,m}$ correlations measured and describe them for each temperature in terms of two states, which we will call S and P , respectively even and odd under R_τ . They appear for n, m both even and both odd. Their physical masses will be denoted M_S and M_P .

We will use in this and the next section either the bare lattice parameters r and β_3 or the physical quantities R and T , which are related to each other by the following equations:

$$RT = r/L_0 \quad (3.6)$$

We show in Fig.3.6 the on-axis correlations $A_{n,m}(r)$, $n \leq m \in [2, 5]$ at $T/T_c = 1.97$ ($\beta_3 = 29$). They are plotted against RT , that is the physical distance in units of the inverse temperature. As expected from general considerations one can see two types of behavior, for the even and odd channels. In the even cases, the three correlations all have the same shape, and they decrease by about one order of magnitude each time two more powers of A are involved. The same is true for the odd cases, with a common decay of the correlations steeper than in the former case (smaller correlation length in lattice units). The overall situation is similar for β_3 higher. For n, m larger than 5, as well as for β_3 very large, the signal/noise ratio becomes very small. This can be understood at the qualitative level by noting that the rescaling Eq.(2.8)

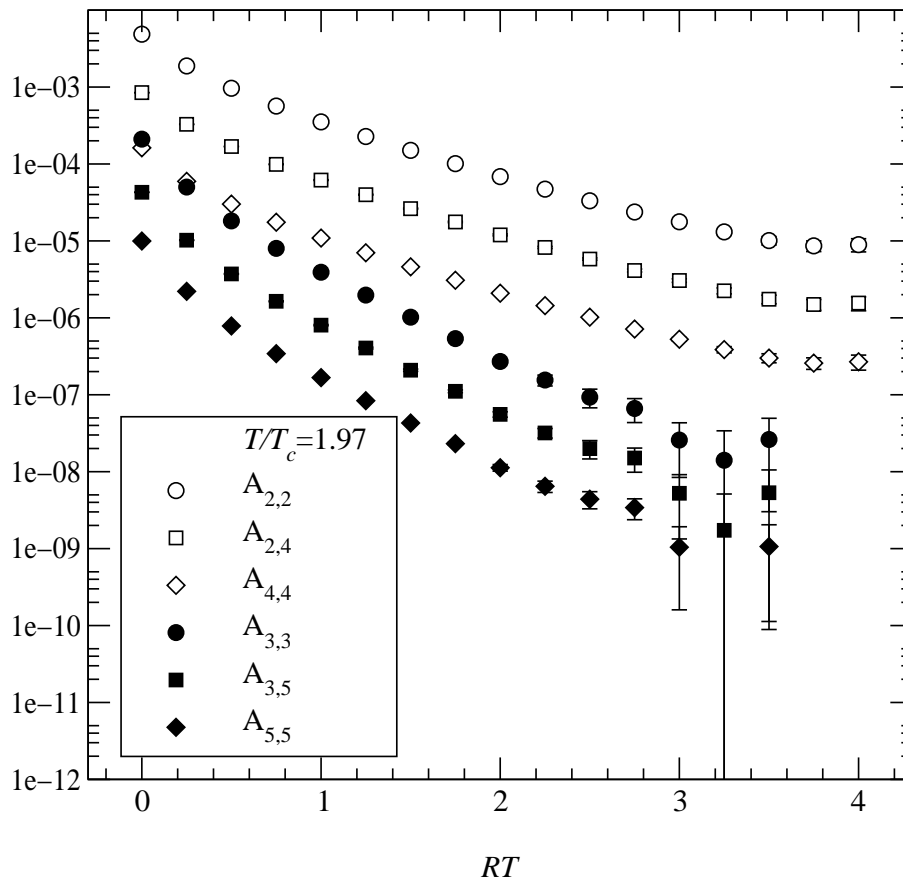


Figure 3.6: The on-axis correlations $A_{n,m}(r)$ at $T/T_c = 1.97$ ($\beta_3 = 29$), versus the distance in units of $1/T$. The even cases $[n, m] = [2, 2], [2, 4]$ and $[4, 4]$ all have the same shape, and the odd cases $[3, 3], [3, 5]$ and $[5, 5]$, again similar with each other in shape, are steeper.

of the A -fields normalizes the kinetic term for the ϕ -fields to the standard, parameter independent form $1/2Tr(D_i\phi)^2$. Hence, if the field renormalization by the interactions is weak, the ϕ correlations should depend only weakly on β_3 , which means that $A_{n,m}$ scales like $\beta_3^{-(n+m)/2}$. This will be illustrated more quantitatively in the next subsection. Due to this scale factor, the A -fields remain “small” in practice down to quite low values of β_3 , which a posteriori explains why the perturbative reduction may still work at a temperature as low as $1.5 T_c$. In fact, we checked that the Polyakov loop correlations are actually fully reconstructed within errors by keeping $\{n, m\}$ up to $\{5, 5\}$ only in their expansion in $A_{n,m}$'s obtained from the small A expansion of (2.31).

Now we want to analyze these $A_{n,m}$ data quantitatively in terms of the lowest states of the spectrum. Let $m_i = a M_i$ be the lowest mass with quantum number $i = S, P$, in lattice units. For particle i with momentum p we introduce a lattice propagator $\tilde{\Delta}_{Latt}(m_i, p)$ in momentum space:

$$\begin{aligned}\tilde{\Delta}_{Latt}^{-1}(m_i, p) &= \hat{p}^2 + 4 \sinh(m_i^2/4), \\ \hat{p}^2 &= 4 \sin^2(p_1/2) + 4 \sin^2(p_2/2).\end{aligned}\tag{3.7}$$

The corresponding contribution to $A_{n,m}(r)$ then reads

$$A_{n,m}(m_i, r) = g_{n,m}^i \frac{1}{L_s^2} \sum_{p_1, p_2} \cos(p_1 r) \tilde{\Delta}_{Latt}(m_i, p),\tag{3.8}$$

where $g_{n,m}^i$ measures the residue of $A_{n,m}$ at the pole of (3.7), which on large enough lattices sits at $p^2 \sim \hat{p}^2 \sim -m_i^2$. With our definitions, $g_{n,m}^i$ is non-zero only for $i = S$ if n and m are even, and for $i = P$ if n and m are odd.

There is a simple result which one may get directly from Eq.(3.8). For the case of the single-particle propagation between two spinless states the residue $g_{n,m}^i$ factorizes (see, for example, [57]):

$$g_{n,m}^i = \gamma_n^i \gamma_m^i\tag{3.9}$$

This property we can probe directly on the correlations since, as r becomes large, it implies

$$X_n \equiv \frac{A_{n,n}(r) A_{n+2,n+2}(r)}{A_{n,n+2}^2(r)} \rightarrow 1.\tag{3.10}$$

We demonstrate this fact for the temperatures $T/T_c = 1.97$ and 5.7 ($\beta_3 = 29$ and 84) on Fig.3.7-3.10. The displayed quantities X_2 and X_3 (symbols \diamond) indeed approach one for the large distances in all cases. However, the quality of the data is poorer for X_3 due to the correlations involving A_5 getting very small.

Similar results are obtained for other values of T/T_c . We thus conclude at this point that a single particle propagation accounts very well for the largest correlation length occurring in each of the two channels. Most of the observed deviations of X_n from one will be interpreted in the next section in terms of the two particle state contributions (symbols \circ in the same figures).

We now proceed to assign values to the two lowest masses M_S and M_P expected from the above findings. This we do by various ways in order to further enforce the statement that the correlations do have the characteristics associated with the pole structure of Eq.(3.7). Down to $r \sim 1$, an excellent approximation to the on-axis correlation (3.8) is given by

$$A_{n,m}(m_i, r) \simeq c \left(\frac{1}{[m_i r]^{1/2}} e^{-m_i r} + \frac{1}{[m_i(L_s - r)]^{1/2}} e^{-m_i(L_s - r)} \right), \quad (3.11)$$

where c is constant in r . The second term takes into account the finite size of the lattice.

We performed fits of this formula to all our $A_{n,m}(r)$ data taken at $r > r_{min}$. These fits are stable with respect to r_{min} , provided it is larger than about 4, and the values found for m_i in different correlations are always consistent with each other. The smallest errors were obtained by using fits to $A_{2,2}$ and $A_{3,3}$ for the reasons described above.

An alternative way for the extracting the effective masses without any fitting is the use of the 0-momentum correlations. They defined for a generic x -space correlation $C(x_1, x_2)$ by

$$C^0(r) = \frac{1}{L_s} \sum_{x_2} C(r, x_2). \quad (3.12)$$

If the lowest mass in C is m , the ansatz (3.7) gives

$$C^0(r) \propto \cosh(m(L_s/2 - r)),$$

and m can be extracted at any r by inverting this relation:

$$m = \log \left(Y(r) + \sqrt{Y^2(r) - 1} \right), \quad (3.13)$$

$$Y(r) = \frac{C^0(r+1) + C^0(r-1)}{2C^0(r)}.$$

As an overall consistency check, we have extracted an effective mass $m^{eff}(r)$ from 0-momentum Polyakov loops correlations (2.31) and compared it to the m_S values obtained by our fits to $A_{2,2}$. We find that $m^{eff}(r)$ is indeed nearly

T/T_c	$M_S/\sqrt{g_3^2 T}$	$M_P/\sqrt{g_3^2 T}$
1.97	1.39(3)	2.51(13)
2.85	1.48(5)	3.02(16)
5.70	1.89(5)	3.22(15)
11.73	2.12(8)	3.44(11)

Table 3.2: Masses in units of $\sqrt{g_3^2 T}$ for the S and P states, as measured from fits to $A_{2,2}$ and $A_{3,3}$ respectively, for different values of T/T_c .

constant, in fact slowly decreasing towards a value compatible with m_S , due to smaller and steeper contributions to (2.31) of the heavier particle P .

We also investigated the D’Hoker’s perturbative scenario, as we have done in Section 2.4.3. Again the largest correlation length in $A_{n,n}$ should be n times shorter than the “Debye screening length”, the inverse of a mass m_E associated with “electric” gluons of the initial (2+1)D model (the scalars of the reduced model). If such was the case, the on-axis correlations $A_{n,n}$ should rather look like

$$A_{n,n}(n m_E, r) \propto \left(\frac{1}{[m_E r]^{1/2}} e^{-m_E r} + \frac{1}{[m_E(L_s - r)]^{1/2}} e^{-m_E(L_s - r)} \right)^n, \quad (3.14)$$

which differs in shape from (3.11), as was illustrated in the previous chapter for the Polyakov loop correlations. We, nevertheless, tried fits with (3.14), but got a definitely worse agreement in the range of temperatures, which we have investigated, i.e. up to $12T_c$. Hence, this scenario is ruled out by the data in this temperature range; if a mass can be defined for the electric gluon in high temperature QCD_3 , it is most probably larger than both $m_S/2$ and $m_P/3$. In the “constituent gluon” picture, as advocated in Ref. [58], one would have bound states instead of a cut. One would, however, expect $m_P/m_S \approx 3/2$.

Our final results for the S and P masses in units of the scale $\sqrt{g_3^2 T}$ are collected in Table 3.2 for the values of T/T_c investigated. They are taken from fits to $A_{2,2}$ and $A_{3,3}$ respectively. The values for M_S agree with those obtained before from the Polyakov loop correlations. As can be seen from the tables, the ratios M_P/M_S vary with T/T_c . There is, however, no clear tendency in the region we have investigated, the ratios being 1.8, 2.0, 1.7, 1.6 in order of increasing temperature. This ratio may, of course, go to 1.5 at still higher temperatures.

3.3 Weak “Strong” Interactions Between Colorless States

Here we will show that even at quite short distances (r small compared to m_S^{-1}) all the condensates $A_n \equiv \langle A_n(x) \rangle$ and correlations $A_{n,m}(r)$ can be reconstructed to a good accuracy from the data for A_2 , $A_{2,2}$ and $A_{3,3}$. The assumption is that the elementary fields $A^\alpha(x)$ (Greek superscripts are color indices) interact only through S and P exchanges between the non-interacting composite $A_2(x)$ and $A_3(x)$, the scale of the fields being fixed by the size of A_2 , while $A_3 = 0$. The details of the derivations are presented in Appendix 3, while here we limit ourselves to the simplest applications and give the results, starting with the local condensates.

3.3.1 Weak Residual Interactions: The A -fields condensates

Since $SU(3)$ has rank 2, any $A_n(x)$ can be reduced to a polynomial in $A_2(x)$ and $A_3(x)$. For n odd A_n is zero by R_τ symmetry. For n even, we apply Wick contraction to all pairs of A^α elementary fields, followed by the meanfield-like substitution

$$A^\alpha(x) A^\beta(x) \rightarrow \frac{1}{4} \delta_{\alpha,\beta} A_2(x). \quad (3.15)$$

As an illustration consider A_4 . With the definitions of Section 3.2, we have

$$2A_4(x) = A_2^2(x) = \frac{1}{2^2} \sum_{\alpha,\beta=1}^8 A^\alpha(x) A^\alpha(x) A^\beta(x) A^\beta(x). \quad (3.16)$$

There we apply (3.15) and then replace $A_2(x)$ by its average A_2 . The $A^\alpha A^\alpha$ and $A^\beta A^\beta$ contractions give $(8 \times A_2/4)^2$, and the additional contributions from $\alpha = \beta$ give $2 \times 8(A_2/4)^2$. Noting that

$$A_{2,2}(0) = \langle A_2^2(x) \rangle - A_2^2 \quad (3.17)$$

(see (3.4)), the net result can be put into two equivalent forms

$$2A_4 = \frac{5}{4} A_2^2, \quad (3.18)$$

$$A_{2,2}(0) = \frac{1}{4} A_2^2. \quad (3.19)$$

This prediction is remarkably well verified in all cases. At $\beta_3 = 29$, the left and right hand sides of (3.19) are respectively $4.86(1) 10^{-3}$ and $4.825(10) 10^{-3}$.

They are $6.093(13) 10^{-4}$ and $6.069(1) 10^{-4}$ at $\beta_3 = 84$. The formula for the $A_{3,3}(0)$ correlations

$$A_{3,3}(0) = \frac{5}{64} A_2^3. \quad (3.20)$$

leads to the similar correspondence. In this case the left and right hand sides are measured to be $2.105(7) 10^{-4}$ and $2.095(6) 10^{-4}$ for $\beta_3 = 29$, $9.365(30) 10^{-6}$ and $9.344(3) 10^{-6}$ for $\beta_3 = 84$. Hence, the effects of residual interactions via higher orders effective couplings in $A_2(x)$ and $A_3(x)$ are less than the percent in the correlations at zero distance.

Before going to the correlations at non-zero distance, let us discuss their normalization, as measured by the values of $A_{2,2}(0)$ and $A_{3,3}(0)$ described just above. At the beginning of the previous section, we argued that the behavior in β_3 , n , m observed for $A_{n,m}$ could follow from the absence of a large renormalization of the ϕ -fields (defined by Eq. (2.8)) by the interactions. Here we note that in the confined phase the effective degrees of freedom are the *massive* composites $\phi_i = Tr \phi^i$, $i = 2, 3$, so that in the limit where they are considered as free fields, one may write (see (3.7))

$$\langle \phi_i(0) \phi_i(0) \rangle \simeq R_i \int d^2 p \frac{1}{\tilde{p}^2 + 4 \sinh(m_i^2/4)}, \quad (3.21)$$

$$\tilde{p}^2 = 4 \sin^2(p_1/2) + 4 \sin^2(p_2/2),$$

the residue R_i being one if neither ϕ nor the composites get renormalized. We computed R_i as the ratio of the l.h.s. of (3.21), directly measured, to the integral in the r.h.s, evaluated numerically on the lattice for the mass values fitted to the correlation data. The result is shown in Fig. 3.11: in the whole temperature range, both residues in the even and odd channels remain uniformly very close to one.

3.3.2 Weak Residual Interactions: Properties of the Correlations

As we have seen in section 3.2 (see Fig. 3.2), the different $A_{n,m}(r)$'s corresponding to the same channel have very similar shapes. Their analysis in terms of one particle exchange was successful, confirmed by the agreement with residue factorization. Nevertheless, although the quantity X_n of Eq. (3.10) does go to one at large distances, it is significantly different from one at medium and short distances (see Figs. 3.7-3.10). We will now show that two particle exchange is responsible for most of this lack of factorization.

The simplest consequence of our assumptions for correlations at finite r is,

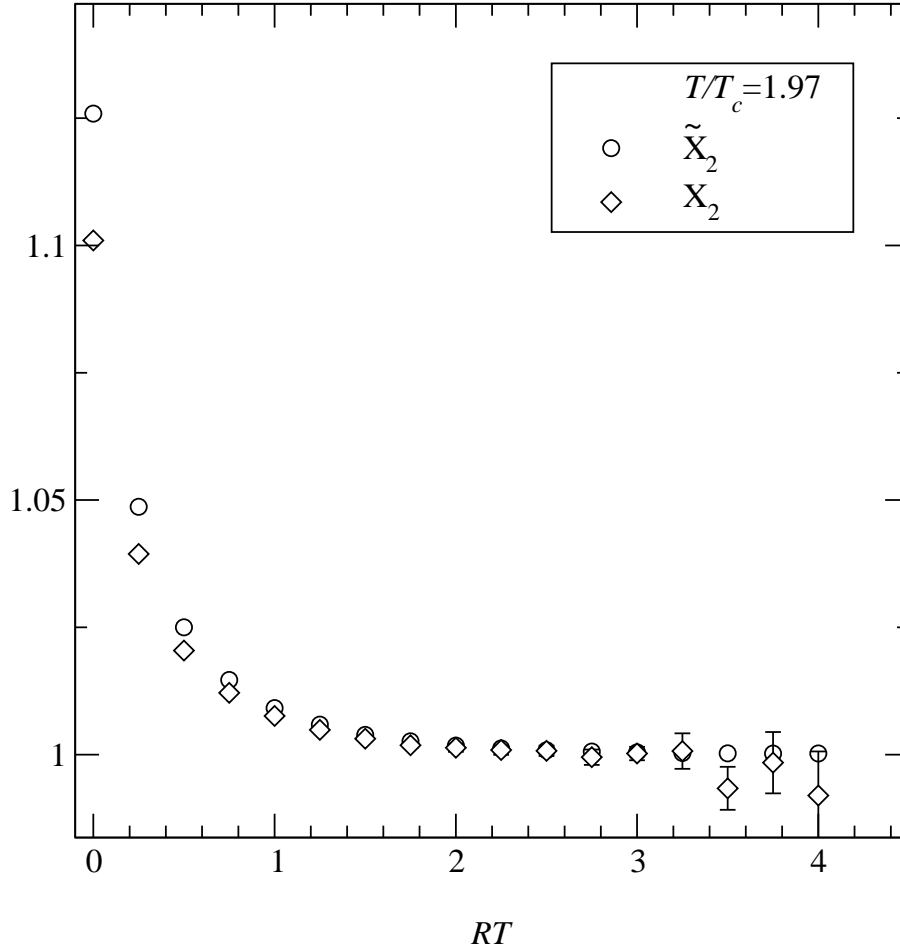


Figure 3.7: Residue factorization: data for the quantity X_2 , Eq. (3.10) at $T/T_c = 1.97$ ($\beta_3 = 29$) versus the distance in units of $1/T$. It approaches one at large distances. The quantity \tilde{X}_2 corresponds to our interpretation (Eq. (3.24)) of the deviation from one of X_2 at shorter distances.

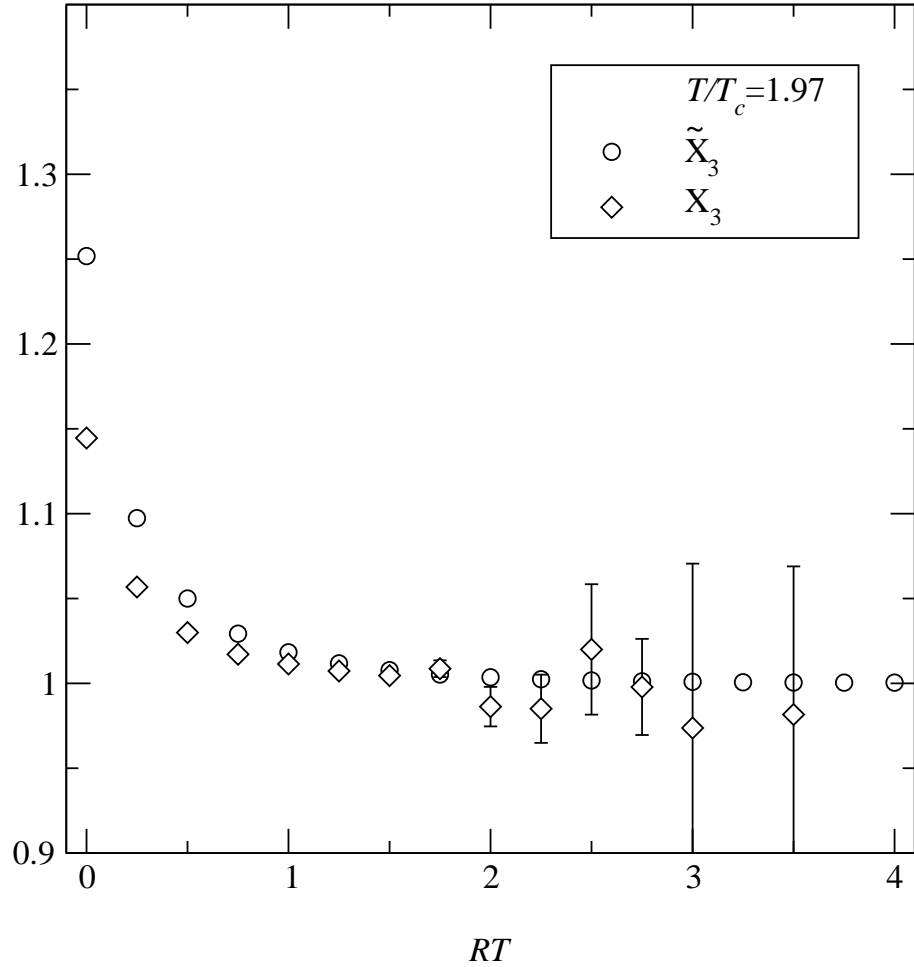


Figure 3.8: Residue factorization: data for the quantity X_3 , Eq. (3.10) $T/T_c = 1.97$ ($\beta_3 = 29$) versus the distance in units of $1/T$. It approaches one at large distances. The quantity \tilde{X}_3 corresponds to our interpretation (Section 4, Eq. (3.25)) of the deviation from one of X_3 at shorter distances.

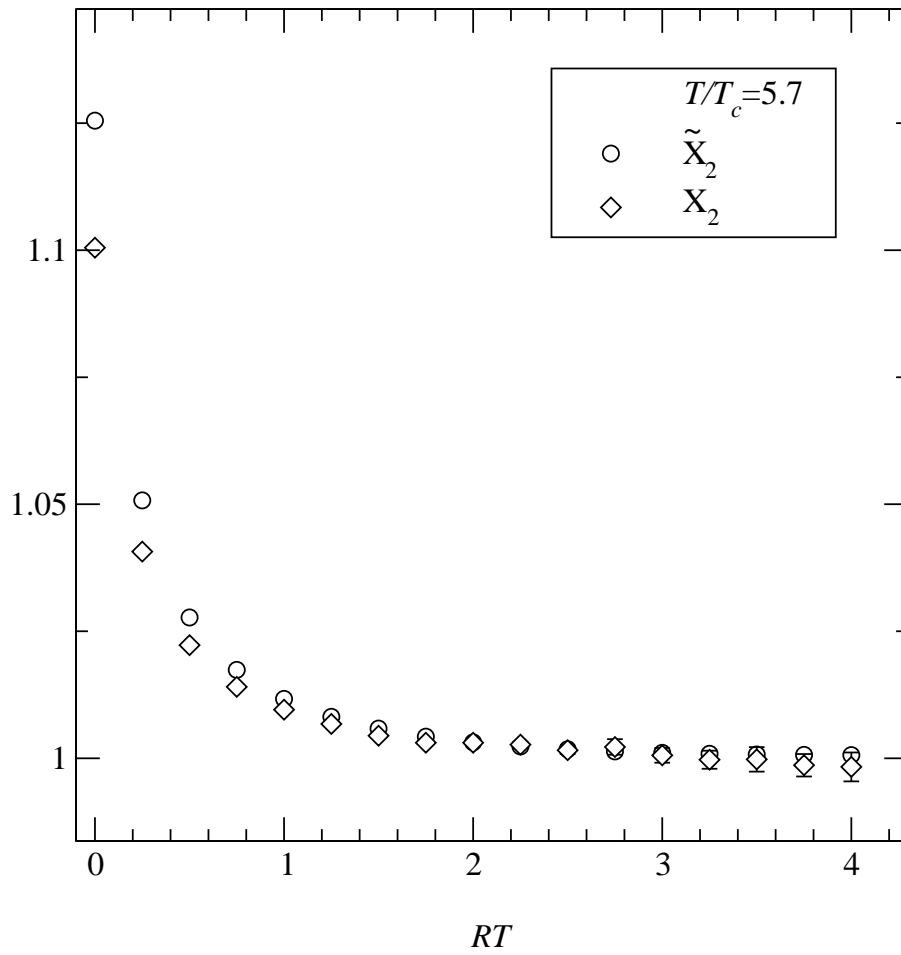


Figure 3.9: Same as in Fig. 3.7 at $T/T_c = 5.7$ ($\beta_3 = 84$).

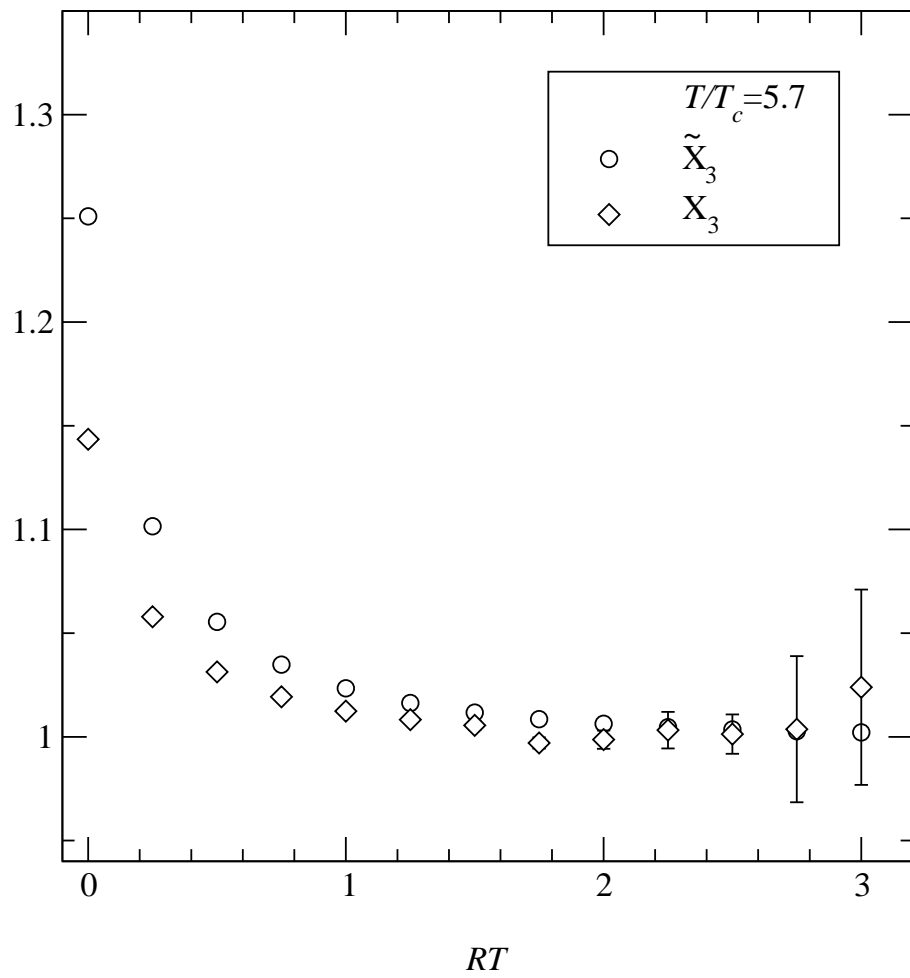


Figure 3.10: Same as in Fig. 3.8 at $T/T_c = 5.7$ ($\beta_3 = 84$).

using Eq.(3.18),

$$A_{2,4}(r) = \frac{5}{4} A_2 A_{2,2}(r), \quad (3.22)$$

which is very well verified at any distance as shown in Fig.3.12 for $T/T_c = 1.97$ ($\beta_3 = 29.0$). A similar agreement is found for the relation

$$A_{3,5}(r) = \frac{35}{24} A_2 A_{3,3}(r), \quad (3.23)$$

derived in the appendix. A new situation arises when we consider $A_{4,4}$, or $A_{5,5}$ where both the initial and final states may couple to a two particle state, (SS) or (SP) respectively. Then the intermediate state in a connected correlation between 0 and r may consist of either one or two particles. For example, to compute $A_{4,4}(r)$, we apply the substitution rule (3.15) to the sum (3.16), and then average using the definitions of $A_{2,2}$ and A_2 . One finds

$$4A_{4,4}(r) = \left(\frac{5}{4}\right)^2 [4A_2^2 A_{2,2}(r) + 2A_{2,2}^2(r)].$$

and

$$A_{5,5}(r) = \left(\frac{35}{24}\right)^2 [A_2^2 A_{3,3}(r) + A_{2,2}(r) A_{3,3}(r)].$$

These both expressions contain two parts. The first term in the square brackets is the contribution of the single particle propagation. The second term is a product of two propagators in space, and is that of a two-particle intermediate state. It provides a correction to exact factorization.

From the definitions Eq.(3.10) of X_2 and X_3 one actually gets the following estimates:

$$X_2(r) \simeq \tilde{X}_2(r) \equiv 1 + \frac{A_{2,2}(r)}{2A_2^2(r)}, \quad (3.24)$$

$$X_3(r) \simeq \tilde{X}_3(r) \equiv 1 + \frac{A_{2,2}(r)}{A_2^2(r)}. \quad (3.25)$$

The estimates $\tilde{X}_2(r)$, $\tilde{X}_3(r)$ are displayed in Figs.3.7-3.8 (resp.3.9-3.10), for comparison with the measured values $X_2(r)$, $X_3(r)$ at $T/T_c = 1.97$ (resp. 5.7), i.e. $\beta_3 = 29.0$ (resp. 84.0). We see that the corrections to factorization implied by the two-particle propagation provide a reasonable explanation of the behavior observed for the X 's at intermediate and short distances. This is especially true in the case of X_2 , showing that there is very little room for contributions from direct non-quadratic couplings in $A_2(x)$ in the full effective action (that resulting from integration over the gauge fields). This justifies our statement that the residual interactions between the colorless boundstates of the adjoint scalars are very weak.

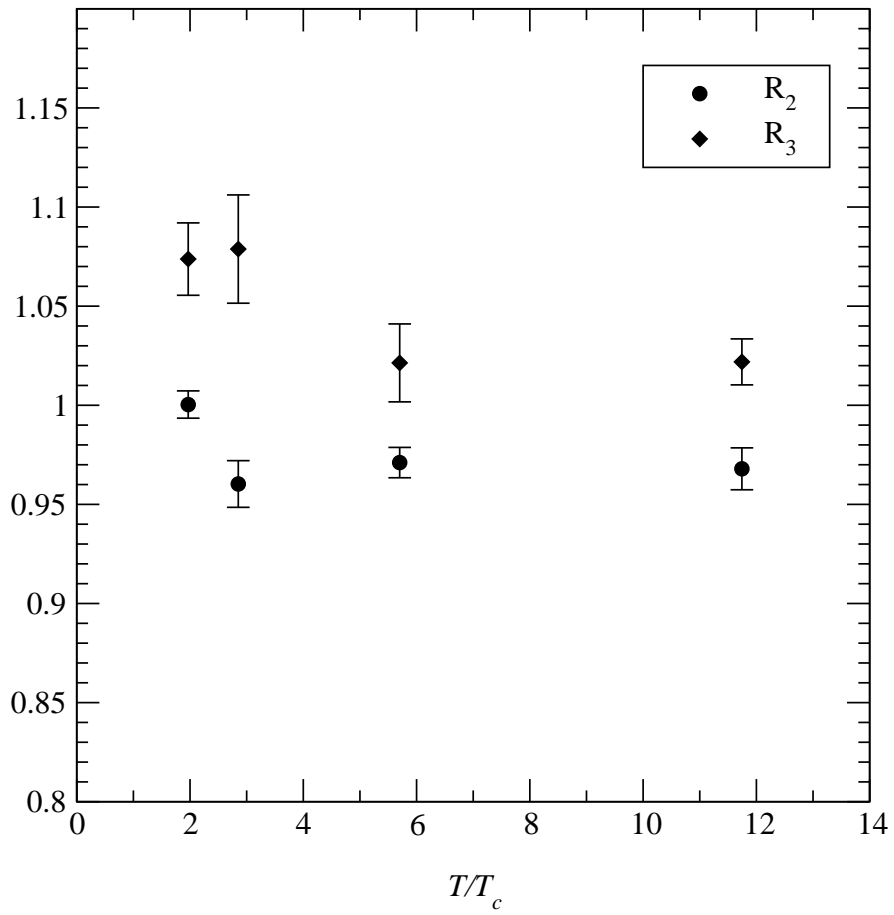


Figure 3.11: The residues R_i defined by Eq. (3.21) stay close to one in the whole temperature range.

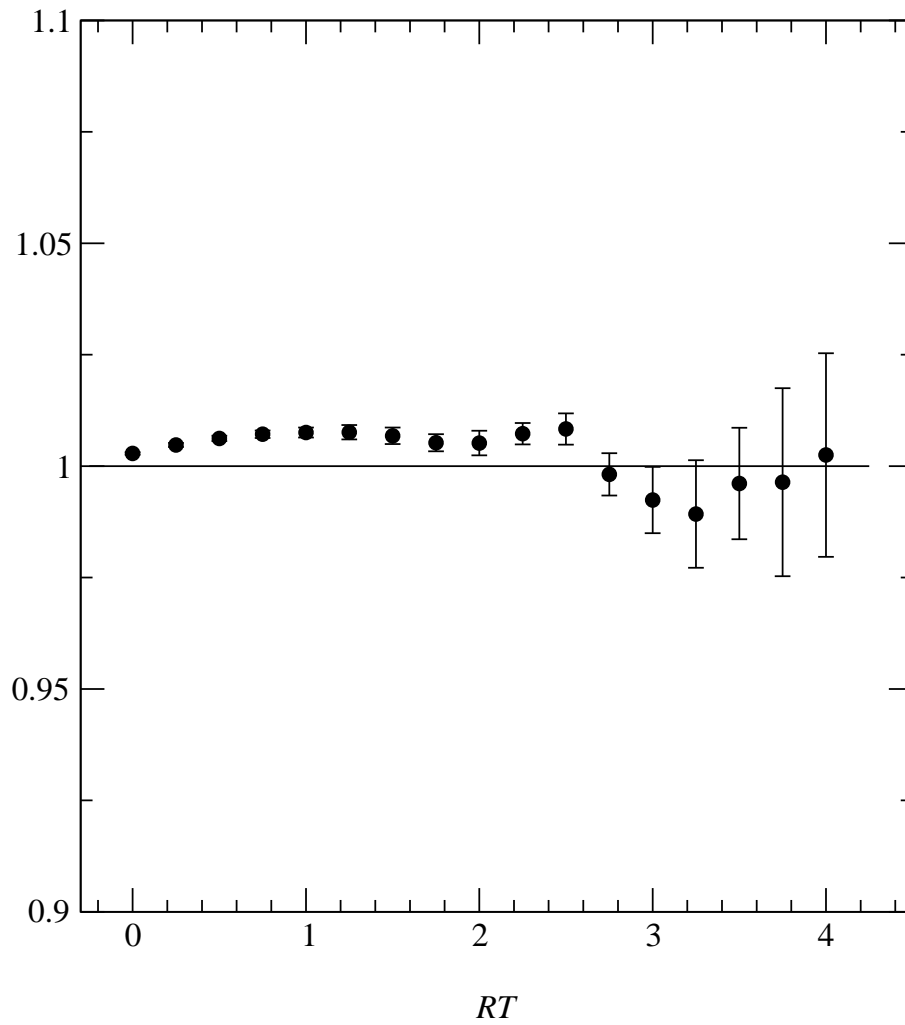


Figure 3.12: Plot of $4A_{24}/5A_2A_{22}$ at $T/T_c = 1.97$ ($\beta_3 = 29$). This quantity is one if Eq. (3.22) exactly holds.

Chapter 4

Z(3) symmetric action

In this chapter we describe an attempt to overcome the absence of the deconfinement phase transition in the model. As we mentioned before, this phenomena is not possible due to the fact that we broke the $Z(3)$ symmetry explicitly when doing the perturbation expansion. One may try to restore this symmetry by hand and derive an effective action possessing it. We will use A_0 variables throughout this chapter, them being a more natural choice for our consideration. The starting point is then:

$$S_{eff}^2(U, A_0) = S_W^2(U) + S_{int}(U, A_0) + S_{pot}(A_0)$$

where $S_W^2(U)$ is the standard Wilson action in two dimensions as defined in Eq.(1.13),

$$S_{int}(U, A_0) = \frac{L_0\beta_3}{6} \sum_x \sum_i Tr [(D_i A_0)^2]$$

$$D_i A_0 = U(x; i) A(x + ai) U(x; i)^{-1} - A(x)$$

$$S_{pot}(A_0) = \sum_x h_2 Tr A_0^2(x) + h_4 (Tr A_0^2(x))^2$$

with couplings

$$h_2 = \frac{9}{16\pi\beta_3}$$

$$h_4 = \frac{9}{\pi L_0\beta_3} \mu$$

$$\mu = \ln L_0 + \frac{5}{2} \ln 2 - 1$$

We may now formulate the basic requirements for this action:

i) should be Z_3 symmetric

- ii) should have also the basic gauge symmetry
- iii) should reproduce the results from the "old" model at the large value of β_3/L_0 , because we need it still for describing the $(2 + 1)$ -dimensional model

One would also like that such a model *predicts* Z_3 -symmetry restoration (reconfinement) as β_3/L_0 (temperature) is lowered. The Polyakov loop should be the order parameter. Close to one (up to a Z_3 phase $\exp(\pm 2\pi i/3)$) at high temperature, it is zero (on the lattice it means - becomes small) in the symmetric phase.

It is obvious that there are infinitely many ways to create the desired action. The most reasonable for us seems the following form:

$$S_{Z_3} = S_W^2(U) + S_{U,V} + S_V \quad (4.1)$$

The plaquette action $S_W^2(U)$ remains untouched. The kinetic term $S_{U,V}$ we

rewrite using the Wilson Lines

$$V(x) = U_0^{L_0}(x) \quad (4.2)$$

where U_0 is the element of the $SU(3)$ group, which we place on every site of our lattice. It relates to the A_0 field as usually via $U_0 = \exp(iA_0)$. The simplest choice for the kinetic term is

$$S_{U,V} \sim \frac{\beta_3}{L_0} \sum_{x,\mu} \left(1 - \frac{1}{3} \Re \text{Tr} U(x; \mu) V(x + a\hat{\mu}) U(x; \mu)^{-1} V^{-1}(x) \right) \quad (4.3)$$

There are two invariants for the $SU(3)$ group, so one can choose any two independent quantities as the basic variables for writing up the potential. We made our choice in favour of the following quantities:

$$O(x) = \frac{1}{3} \text{Tr} V(x) \quad O^*(x) = \frac{1}{3} \text{Tr} V^*(x) \quad (4.4)$$

that is the Polyakov loop and its conjugate. This choice of variables leads to the following considerations

- gauge invariance implies that S_V^R depends only on the set of all pairs $\{O(x), O^*(x)\}$
- by Z_3 invariance, the lowest degree *local* monomial in O, O^* is $O_2(x) = O(x)O^*(x)$ (degree two).

- next terms should be $O^3(x)$ and $O^{*3}(x)$ *with degree three*, there is no reason for them to be absent. They are independent degrees of freedom
- reality implies that at order 3 in O the local action depends only on

$$O_3(x) = \frac{1}{2}(O^3 + O^{*3}).$$

and terms proportional to it are expected on very general grounds in the full effective Polyakov loop potential.

The simplest form of such potential is then

$$S_V = \sum_{x \in \Lambda_2} (\lambda_2 |O(x)|^2 + \lambda_3 \text{Re}(O^3(x))) \quad (4.5)$$

The corresponding couplings λ_2 and λ_3 have to be fixed by again matching the small A_0 expansion of (4.1) to S_{A_0} . Although this proposal still contains a substantial amount of arbitrariness, the following may be stated:

- i) All desired symmetries are implemented,
- ii) All independent degrees of freedom are involved,
- iii) In the region of phase space where the O 's are close to one, the action looks like the old one. The hope is that it is the relevant region at *large* β_3/L_0 values,
- iv) In the region of phase space where the O 's are close to zero, the action is truncated to the two lowest degree monomials in O, O^* , that is two and three, not two and four. The hope is that it is the relevant region at *low* β_3/L_0 values.

The other option would be to ignore the requirements ii) and iv) and use instead of $\Re(O^3(x))$ the term with $O^4(x)$. This way it is also possible to match all the terms of the potential (see below).

One wants to be working in the unbroken phase, and assume that $\text{tr} A^3 = 0$. The obvious choice for the kinetic term is

$$S_I = \frac{\beta_3}{6L_0} \sum (1 - \text{Re} \text{Tr} \{U(x, -\mu) O(x + \mu) U^\dagger(x, \mu) O^*(x + \mu)\})$$

Expanding the action (4.5) one easily gets:

$$\lambda_2^c = \frac{9}{16} \frac{20\mu - 1}{\pi L_0^2}$$

$$\lambda_3^c = -\frac{3}{8} \frac{12\mu - 1}{\pi L_0^2}$$

Here is the table for the coefficients for $\beta_3 = 29$:

L_0	λ_2^c	λ_3^c
4	0.4631026079	-0.182256888
8	0.1545592536	-0.06107766263

The model described above represents a good candidate for the improved effective model, which can allow us to calculate the three-dimensional quantities closer to the phase transition. Our test runs indicate that this model does have the second order phase transition in β_2 with Polyakov loop being an order parameter. However, it still requires a detailed study, which goes beyond the scope of the current work.

Chapter 5

Conclusions and outlook

This work is the detailed investigation of the dimensional reduction for SU(3) gauge theory in (2+1)-dimensions at high temperature. We have produced an effective reduced model for the static variables following [14, 15, 16]. This means that the integration over the non-static modes has been performed perturbatively, and the effective couplings have been kept to one loop order for the two point and four point functions. Higher order contributions, neglecting which was a part of our approximation, are unimportant at large distances and high temperatures.

We investigated the validity of this approximation for the correlation function between Polyakov loops and corresponding screening masses, as well as the spatial string tension. For the (2+1)-dimensional theory and the corresponding 2-dimensional reduced adjoint Higgs-gauge model we were able to obtain very precise numerical results. Therefore, we could make a detailed comparison, including a scaling analysis, which strongly supports the assumption that our lattices correspond to a large enough value of the temporal extent L_0 .

For the correlation between Polyakov loops the dimensional reduction works very well down to temperatures of the order of $1.5T_c$, where T_c is the critical temperature of the deconfinement phase transition of the original model. This is true even at distances down to or below $1/T$. And it does even better than in the (3+1)-dimensional case. The correlation between Polyakov loops is well described by a simple pole in momentum space, even at high temperatures. This situation is not manifested in (3+1)-dimensional theory where at high temperatures the data favour the exchange of two Debye screened gluons [43, 29, 33, 44]. The disagreement may be related to the stronger infrared divergences in (2+1) dimensions, which invalidate the perturbatively resummed Debye screening picture. A further investigation of this behavior in (3+1) dimensions would certainly be very interesting.

The spatial Wilson loops in (2+1) dimensions do not correspond to a static

operator and is not reproduced at all by itself. However, for the string tension, which is extracted from Wilson loops of extent larger than $1/T$, one can hope that the non-static corrections are small. Our comparison favours this situation. In fact, the Higgs sector seems to have little influence on the value of the string tension; there is a fairly good agreement also with the analytically solvable pure two-dimensional gauge theory where confinement is given by the two-dimensional Coulomb potential. The differences between the string tension in the three cases considered are of the order of a few percent. To make a definite statement if these differences are real continuum effects, one must further study finite size and scaling corrections.

Our work shows that it may be possible to explain the non-perturbative features of (2+1)-dimensional QCD in the deconfined phase with a relatively simple two-dimensional model. The model possesses, however, a non-physical phase transition associated with the symmetry of the Higgs field sign reversal R_τ , which corresponds to the time reversal of the original model. The reduced values of the Higgs potential are in the non-physical broken phase. However, we are able to simulate with these values in the metastable phase, and never drop into the broken one on sufficiently large lattices due to this transition being strongly first order.

We studied the reduced model in the region of the unbroken symmetry to identify two boundstates S and P , respectively, even and odd under R_τ and thus coupled to monomials, respectively, of degree $2n$ and $2n + 1$ in the higgs field. The S signal coincides with that previously obtained from the Polyakov loops correlations, where, however, the P -state contributions could not be disentangled. These results came from the measurement of three even–even and three odd–odd distinct correlations, as functions of the on-axis lattice distance r . We very carefully analyzed their shape in r , with the result that in all cases the signal found was that expected from the occurrence of genuine poles in momentum space. Our data invalidated the D’Hoker’s scenario where the decay of such correlations with the distance reflects the propagation in $3D$ of $p = 2n$ or $2n + 1$ “electric gluons”. In other words, the perturbative result that the correlation length equals to $1/p$ times the “Debye screening length” is inadequate in the present case.

By comparing the size of the three different correlations measured for each of the S and P sectors, we were able to show that residue factorization holds, as expected on general grounds when one particle propagates between different states. The agreement with factorization was expectedly found to be particularly good at large distances. We were also able to demonstrate that deviations at shorter distances are to a large extent compatible with propagation of two particles, namely two S or S and P , respectively, in the S or P channel. We

thus make a conclusion that the scalar sector of the reduced model at large distance can be described by the two weakly interacting colorless states.

The perturbative approach used to derive the reduced model explicitly broke the $Z(3)$ symmetry of the (2+1) dimensional system, thus we do not have the phase transition which would correspond to the deconfinement phase transition of the original model. We presented here a candidate for the effective model, based on the original spatial gauge variables and Wilson Lines. This model is likely not only to be able to reproduce the full model at high temperature but also exhibits a deconfinement-like phase transition with Polyakov loop being an order parameter. Careful study of this model is needed to make a definite statement.

Farther interesting topics for investigations are of course more real-world models. The similarly detailed analysis for pure gauge QCD in (3 + 1)D would be interesting, with extending to the full QCD with dynamic fermions. Furthermore, the study of thermodynamical quantities like pressure and entropy may be of interest, as well as study of the operators which are even and odd under other symmetries of the model - space reversal and charge conjugation.

Chapter 6

Acknowledgements

At this point I would like to thank everybody, who during these years supported me at my work and made it possible. At first, of course, my supervisor Bengt Petersson, who with infinite patience guided me through the process of learning, while giving me as much freedom as I could digest. I am really happy to have you as a supervisor, Bengt.

I also would like to thank the Bielefeld particle physics group for having so much of different activities going on and providing a real atmosphere of high-end physics, which is very motivating and inspiring. Also thanks go to our collaborators: Andre Morel, who made me more disciplined in presentation of the results and supported my interest in analytic calculations; Thomas Reisz and Piotr Bialas - for having an immense influence on me in analytical and numerical sides of physics respectively.

It would be impossible not to mention Gena Zinovjev, the supervisor of my diploma work - who invested a lot of effort to make it all happened and supported me in my scientific career.

The last but not the least I would like to thank our secretaries - Susi von Reder, and most of all - Gudrun Eickmeyer who made my life here as uncomplicated as it could be, helping me with all the administrative things and guiding me through the dark forests of german, ukrainian and american bureaucracy.

I dedicate this work to my parents - my mother Maria and my father Vladimir - for combination of freedom and support in whatever I was doing, which is really invaluable and my wife Jenny - for becoming such despite my doing this Ph.D. thesis.

Finally I would like to thank DFG and DAAD for supporting this work financially.

Appendix A

Appendix

A.1 General $SU(3)$ formulae and definitions

In this Appendix we present the formulae and definitions which will be used in the following calculations.

The Gell-Mann matrices are:

$$\begin{aligned}\lambda_1 &= \begin{pmatrix} 0 & 1 & 0 \\ 1 & 0 & 0 \\ 0 & 0 & 0 \end{pmatrix} & \lambda_2 &= \begin{pmatrix} 0 & -i & 0 \\ i & 0 & 0 \\ 0 & 0 & 0 \end{pmatrix} & \lambda_3 &= \begin{pmatrix} 1 & 0 & 0 \\ 0 & -1 & 0 \\ 0 & 0 & 0 \end{pmatrix} & (A.1) \\ \lambda_4 &= \begin{pmatrix} 0 & 0 & 1 \\ 0 & 0 & 0 \\ 1 & 0 & 0 \end{pmatrix} & \lambda_5 &= \begin{pmatrix} 0 & 0 & -i \\ 0 & 0 & 0 \\ i & 0 & 0 \end{pmatrix} & \lambda_6 &= \begin{pmatrix} 0 & 0 & 0 \\ 0 & 0 & 1 \\ 0 & 1 & 0 \end{pmatrix} \\ \lambda_7 &= \begin{pmatrix} 0 & 0 & 0 \\ 0 & 0 & -i \\ 0 & i & 0 \end{pmatrix} & \lambda_8 &= \frac{1}{\sqrt{3}} \begin{pmatrix} 1 & 0 & 0 \\ 0 & 1 & 0 \\ 0 & 0 & -2 \end{pmatrix}\end{aligned}$$

The actual generators of the $SU(3)$ group/algebra we take as the half of the lambda-matrices

$$T_a \equiv \frac{1}{2}\lambda_a \quad (A.2)$$

They satisfy (for any $SU(N)$ group) the following commutation/anticommutation relations:

$$[T_a T_b] = i f_{abc} T_c \quad (A.3)$$

$$\{T_a T_b\} = \frac{4}{N} \delta_{ab} I_N + 4 d_{abc} T_c \quad (A.4)$$

with f_{abc} being the absolutely antisymmetric and d_{abc} - absolutely symmetric tensors of the third rank. Traces of the generators and their products satisfy the following relations:

$$TrT_a = 0 \quad (\text{A.5})$$

$$TrT_aT_b = \frac{1}{2}\delta_{ab} \quad (\text{A.6})$$

$$TrT_aT_bT_c = \frac{1}{4}(d_{abc} + if_{abc}) \quad (\text{A.7})$$

$$TrT_aT_bT_aT_c = -\frac{1}{4N}\delta_{bc} \quad (\text{A.8})$$

Also

$$T_aT_b = \frac{1}{2} \left[\frac{1}{N}\delta_{ab} + (d_{abc} + if_{abc})T_c \right] \quad (\text{A.9})$$

$$T_a^{ij}T_a^{kl} = \frac{1}{2} \left(\delta_{il}\delta_{kj} - \frac{1}{N}\delta_{ij}\delta_{kl} \right) \quad (\text{A.10})$$

Structure constants of the group satisfy the Jacobi identities

$$f_{abc}f_{ecd} + f_{cbe}f_{aed} + f_{dbe}f_{ace} = 0 \quad (\text{A.11})$$

$$f_{abc}f_{ecd} + f_{cbe}d_{aed} + f_{dbe}d_{ace} = 0 \quad (\text{A.12})$$

From the antisymmetric nature of the f_{abc} directly follows

$$f_{abb} = 0$$

for any b . Similar self-contraction relation holds for d_{abc} , where we put the explicit summation to distinguish it from the previous formula.

$$\sum_b d_{abb} = 0$$

The contraction relations for f and d are

$$f_{acd}f_{bcd} = N\delta_{ab} \quad (\text{A.13})$$

$$d_{acd}d_{bcd} = \frac{N^2 - 4}{N}\delta_{ab} \quad (\text{A.14})$$

A.2 One Link Integral

We will use here the Gell-Mann parametrization of the arbitrary $SU(3)$ matrix:

$$U = e^{i\frac{\alpha_i\lambda_i}{2}} \quad (\text{A.15})$$

$$U^\dagger = e^{-i\frac{\alpha_i\lambda_i}{2}} \quad (\text{A.16})$$

where λ_i are the Gell-Mann matrices (A.1). For small α_i we can expand

$$\begin{aligned} U &\sim 1 + i\frac{\alpha_i\lambda_i}{2} - \frac{\alpha_i\alpha_j\lambda_i\lambda_j}{8} - i\frac{\alpha_i\alpha_j\alpha_k\lambda_i\lambda_j\lambda_k}{8 \cdot 3!} \\ U^\dagger &\sim 1 - i\frac{\alpha_i\lambda_i}{2} - \frac{\alpha_i\alpha_j\lambda_i\lambda_j}{8} + i\frac{\alpha_i\alpha_j\alpha_k\lambda_i\lambda_j\lambda_k}{8 \cdot 3!} \end{aligned} \quad (\text{A.17})$$

Let us calculate the measure first. Following the standard procedure we calculate differentials:

$$\begin{aligned} dU &\sim i\frac{d\alpha_i\lambda_i}{2} - \frac{(d\alpha_i\alpha_j + \alpha_id\alpha_j)\lambda_i\lambda_j}{8} - i\frac{(d\alpha_i\alpha_j\alpha_k + \alpha_id\alpha_j\alpha_k + \alpha_i\alpha_jd\alpha_k)\lambda_i\lambda_j\lambda_k}{8 \cdot 3!} = \\ &= i\frac{d\alpha_i\lambda_i}{2} - \frac{d\alpha_i\alpha_j(\lambda_i\lambda_j + \lambda_j\lambda_i)}{8} - i\frac{d\alpha_i\alpha_j\alpha_k(\lambda_i\lambda_j\lambda_k + \lambda_j\lambda_i\lambda_k + \lambda_k\lambda_j\lambda_i)}{8 \cdot 3!} = \\ &= i\frac{d\alpha_iF_i}{2} - \frac{d\alpha_i\alpha_jF_{ij}}{8} - i\frac{d\alpha_i\alpha_j\alpha_kF_{ijk}}{8 \cdot 3!} \\ dU^\dagger &= -i\frac{d\alpha_iF_i}{2} - \frac{d\alpha_i\alpha_jF_{ij}}{8} + i\frac{d\alpha_i\alpha_j\alpha_kF_{ijk}}{8 \cdot 3!} \end{aligned}$$

Now we calculate the "metric tensor" in this parametrization:

$$\begin{aligned} \text{Tr}dUdU^\dagger &\sim \text{Tr} \left(i\frac{d\alpha_iF_i}{2} - \frac{d\alpha_i\alpha_jF_{ij}}{8} - i\frac{d\alpha_i\alpha_j\alpha_kF_{ijk}}{8 \cdot 3!} \right) \times \\ &\times \left(-i\frac{d\alpha_aF_a}{2} - \frac{d\alpha_a\alpha_bF_{ab}}{8} + i\frac{d\alpha_a\alpha_b\alpha_cF_{abc}}{8 \cdot 3!} \right) \\ &= \text{Tr} \frac{d\alpha_iF_i}{2} \frac{d\alpha_aF_a}{2} + \frac{d\alpha_i\alpha_jF_{ij}}{8} \frac{d\alpha_a\alpha_bF_{ab}}{8} - 2\frac{d\alpha_iF_i}{2} \frac{d\alpha_a\alpha_b\alpha_cF_{abc}}{8 \cdot 3!} \\ &\equiv g_{ia}d\alpha_id\alpha_a \end{aligned} \quad (\text{A.18})$$

with

$$\begin{aligned} g_{ia} &\equiv \frac{\text{Tr}F_iF_a}{2^2} + \frac{\alpha_j\alpha_b\text{Tr}F_{ij}F_{ab}}{2^2(2 \times 2!)^2} - 2\frac{\alpha_b\alpha_c\text{Tr}F_iF_{abc}}{2^2 \times 2^2 \cdot 3!} = \\ &= \frac{\delta_{ia}}{2} + \frac{\alpha_j\alpha_b\text{Tr}F_{ij}F_{ab}}{64} - \frac{\alpha_b\alpha_c\text{Tr}F_iF_{abc}}{8 \cdot 3!} \end{aligned} \quad (\text{A.19})$$

$$q_{il} = 2g_{il} = 1 + \alpha_j \alpha_k \left(\frac{\text{Tr} F_{ij} F_{lk}}{32} - \frac{\text{Tr} F_i F_{lkj}}{24} \right) \quad (\text{A.20})$$

According to [48] the invariant measure is then

$$d\mu = \sqrt{\det g} \prod_i d\alpha_i \quad (\text{A.21})$$

Using the following representation of the determinant

$$\det q_{il} = \exp \text{Tr} \log q_{il}$$

$$\log q_{il} = \alpha_j \alpha_k \left(\frac{\text{Tr} F_{ij} F_{lk}}{32} - \frac{\text{Tr} F_i F_{lkj}}{24} \right) \quad (\text{A.22})$$

$$\text{Tr} \log q_{il} = \sum_i \alpha_j \alpha_k \left(\frac{\text{Tr} F_{ij} F_{ik}}{32} - \frac{\text{Tr} F_i F_{ikj}}{24} \right) \equiv \alpha_j \alpha_k T_{jk} \quad (\text{A.23})$$

where we defined (and calculated)

$$T_{jk} = \sum_i \left(\frac{\text{Tr} F_{ij} F_{ik}}{32} - \frac{\text{Tr} F_i F_{ikj}}{24} \right) = -\frac{1}{4} \delta_{jk}$$

So the expression for the measure takes the following simple form

$$d\mu = \sqrt{\det g} \prod_i d\alpha_i = C e^{-\frac{1}{8} \alpha_i \alpha_i} \prod_i d\alpha_i \quad (\text{A.24})$$

We also define

$$G_{ijkl} = \text{Tr} \lambda_i \lambda_j \lambda_k \lambda_l$$

Explicit calculation leads to:

$$G_{ijkl} \alpha_i \alpha_j \alpha_k \alpha_l = 2 \sum_{i,j} a_i^2 a_j^2$$

Now let us define the following average

$$\langle A \rangle_\gamma = \int_{-\infty}^{\infty} \prod d\alpha_i A \exp(-\gamma a_i a_i) \quad (\text{A.25})$$

We will need these averages:

$$\langle 1 \rangle_\gamma = \frac{\pi^4}{\gamma^4}; \quad \langle a_i^2 a_j^2 \rangle_\gamma = \frac{\pi^4}{4\gamma^6}; \quad \langle a_i^4 \rangle_\gamma = \frac{3\pi^4}{4\gamma^6}$$

$$\left\langle \sum_{i,j} a_i^2 a_j^2 \right\rangle_{\gamma} = (8 * 8 - 8) \langle a_i^2 a_j^2 \rangle_{\gamma} + 8 \langle a_i^4 \rangle_{\gamma} = 20 \frac{\pi^4}{\gamma^6} \quad (\text{A.26})$$

Now we can calculate the statistical sum:

$$\begin{aligned} Z &= \int d\mu e^{\frac{\beta}{2N} \text{Tr}(U+U^\dagger)} = e^{\beta} \int d\mu e^{-\frac{\beta}{2N} (\text{Tr}(1-U) + \text{Tr}(1-U^\dagger))} = \\ &= C e^{\beta} \int e^{\alpha_j \alpha_k T_{jk}} e^{-\frac{\beta}{2N} \left(\frac{\alpha_i \alpha_i \delta_{ij}}{2} - \frac{\alpha_i \alpha_j \alpha_k \alpha_l \text{Tr} \lambda_i \lambda_j \lambda_k \lambda_l}{8 \cdot 4!} \right)} = \\ &= C e^{\beta} \int e^{-\left(\alpha_i \alpha_i \left[\frac{\beta}{4N} \delta_{ij} + \frac{1}{8} \delta_{ij} \right] - \frac{\beta}{2N} \frac{\alpha_i \alpha_j \alpha_k \alpha_l G_{ijkl}}{8 \cdot 4!} \right)} = \end{aligned} \quad (\text{A.27})$$

Defining the new coupling

$$\gamma = \left(\frac{\beta}{4N} + \frac{1}{8} \right) \quad (\text{A.28})$$

and expanding the integrand we get

$$Z = C e^{\beta} \int e^{-\alpha_i \alpha_i \gamma \delta_{ij}} \left[1 + \frac{\beta}{2N} \frac{G_{ijkl}}{8 \cdot 4!} \alpha_i \alpha_j \alpha_k \alpha_l \right] \quad (\text{A.29})$$

Now we will use the formulae for the averages (A.26) and get

$$Z = C e^{\beta} \frac{\pi^4}{\left(\frac{\beta}{4N} + \frac{1}{8} \right)^4} \left[1 + \frac{\beta}{2N} \frac{20}{96 \left(\frac{\beta}{4N} + \frac{1}{8} \right)^2} \right] \quad (\text{A.30})$$

At this point we set $N = 3$ (in fact our derivation is not for arbitrary N at this point, but we kept it variable for transparency) and obtain for the string tension

$$\begin{aligned} \sigma &= - \ln \frac{\partial \ln \left(C e^{\beta} \frac{\pi^4}{\left(\frac{\beta}{12} + \frac{1}{8} \right)^4} \left[1 + \frac{\beta}{6} \frac{20}{96 \left(\frac{\beta}{12} + \frac{1}{8} \right)^2} \right] \right)}{\partial \beta} = \\ &= - \ln \frac{\partial \left(\beta - 4 \ln(2\beta + 3) + \ln \left(1 + 20 \frac{\beta}{(2\beta+3)^2} \right) \right)}{\partial \beta} \\ &= - \ln \left(1 - \frac{8}{2\beta + 3} + \frac{\frac{20}{(2\beta+3)^2} - 80 \frac{\beta}{(2\beta+3)^3}}{1 + 20 \frac{\beta}{(2\beta+3)^2}} \right) \end{aligned} \quad (\text{A.31})$$

and expanding to the second order in $1/\beta$ we arrive to the final answer:

$$\sigma = \frac{4}{\beta} + \frac{7}{\beta^2} + O\left(\frac{1}{\beta^3}\right) \quad (\text{A.32})$$



Figure A.1: Feynman diagrams for the second order term in the potential

A.3 One-loop Feynman diagrams for the vacuum polarization

Here we calculate the Feynman diagrams for the $\tilde{\Pi}_{00}^{ns}$. We define the following variables:

$$\hat{q}_\mu = 2 \sin \frac{q_\mu}{2} \quad (\text{A.33})$$

$$c_{q_\mu} = \cos \frac{q_\mu}{2} \quad (\text{A.34})$$

$$\hat{\mathbf{q}}^2 = \hat{q}^2 + \hat{q}_0^2 = \sum_{m=0}^3 \hat{q}_m \hat{q}_m \quad (\text{A.35})$$

$$\hat{q}^2 = \sum_{m=1}^3 \hat{q}_m \hat{q}_m \quad (\text{A.36})$$

Feynman rules we need are [30]:

1. 3-line vertex: $(a, p, \mu) (b, q, \nu) (c, k, \lambda)$ gives factor

$$ig f^{abc} \left[\delta_{\lambda\nu} (k - q)_\mu c_{p\nu} + \delta_{\lambda\mu} (p - k)_\nu c_{q\lambda} + \delta_{\nu\mu} (q - p)_\lambda c_{k\mu} \right] \quad (\text{A.37})$$

2. propagator $(a, i)[q](b, j)$ gives factor

$$D_{ij}^{ab}(q) = \frac{1}{\hat{q}^2} \left(\delta_{ij} - \frac{\hat{q}_i \hat{q}_j}{\hat{\mathbf{q}}^2} \right) + \frac{\hat{q}_i \hat{q}_j}{\hat{\mathbf{q}}^2} \left(\frac{1}{\hat{q}_0^2} (1 - \delta_{q_0,0}) + \alpha \frac{\delta_{q_0,0}}{\hat{\mathbf{q}}^2} \right) \quad (\text{A.38})$$

$$D_{00}^{ab}(q) = \frac{\delta^{ab} \delta_{q_0,0}}{\hat{\mathbf{q}}^2} \quad (\text{A.39})$$

Non-static part is

$$D_{ij}^{ab}(q) = \frac{1}{\hat{q}^2} \left(\delta_{ij} - \frac{\hat{q}_i \hat{q}_j}{\hat{\mathbf{q}}^2} \right) + \frac{\hat{q}_i \hat{q}_j}{\hat{\mathbf{q}}^2} \left(\frac{1}{\hat{q}_0^2} \right) \quad (\text{A.40})$$

$$D_{00}^{ab}(q) = 0 \quad (\text{A.41})$$

First diagram

The first diagram (Fig.A.1, left) has two internal lines and two vertices, that is

$$(a, q, \mu) (d, q' - k, \lambda) (c, -q', \rho) \text{ and } (c, q', \sigma) (d, q - q', \tau) (b, -q, \nu)$$

Hence, according to the Feynman rules above we have

$$\begin{aligned} Q_1(q) &= \frac{1}{L^2 L_0} \sum \left(\frac{i}{\sqrt{2c_f}} \right)^2 \tilde{D}_{\lambda\tau}^{dd}(q' - q) \tilde{D}_{\rho\sigma}^{cc}(q') \times \\ &\times f^{adc} \left[\delta_{\lambda\rho} (-q' + q - q')_\mu c_{q_\lambda} + \delta_{\mu\rho} (q + q')_\lambda c_{(q'-q)_\rho} + \delta_{\lambda\mu} (q' - 2q)_\rho c_{q'_\mu} \right] \times \\ &\times f^{cdb} \left[\delta_{\tau\nu} (-q + q' - q)_\sigma c_{q'_\tau} + \delta_{\sigma\nu} (q + q')_\tau c_{(q'-q)_\nu} + \delta_{\sigma\tau} (q - 2q')_\nu c_{q_\sigma} \right] \end{aligned} \quad (\text{A.42})$$

Now we set $\mu = \nu = 0$, and we calculate for $q = 0$

$$\begin{aligned} Q_1(0) &= \frac{1}{L_s^2 L_0} \sum \left(\frac{i}{\sqrt{2c_f}} \right)^2 \tilde{D}_{\lambda\tau}^{dd}(q') \tilde{D}_{\rho\sigma}^{cc}(q') \times \\ &\times f^{adc} \times \left[\delta_{\lambda\rho} (-2q')_0 + \delta_{0\rho} (q')_\lambda c_{q'_0} + \delta_{\lambda 0} (q')_\rho c_{q'_0} \right] \\ &\times f^{cdb} \left[\delta_{\tau 0} (q')_\sigma c_{q'_0} + \delta_{\sigma 0} (q')_\tau c_{q'_0} + \delta_{\sigma\tau} (-2q')_0 \right] \end{aligned} \quad (\text{A.43})$$

Only the first term in the first bracket and the last term in the second survive

$$Q_1(0) = \frac{1}{L_s^2 L_0} \sum \left(\frac{i}{\sqrt{2c_f}} \right)^2 f^{adc} f^{cdb} (\tilde{D}_{ij}^{dd}(q') \tilde{D}_{ij}^{cc}(q') (-2q')_0 (-2q')_0) \quad (\text{A.44})$$

Now we insert the propagators and omit the prime

$$Q_1(0) = \frac{1}{L_s^2 L_0} \sum \left(\frac{i}{\sqrt{2c_f}} \right)^2 f^{adc} f^{cdb} \left(\frac{1}{\hat{q}^2} \left(\delta_{ij} - \frac{\hat{q}_i \hat{q}_j}{\hat{\mathbf{q}}^2} \right) + \frac{\hat{q}_i \hat{q}_j}{\hat{\mathbf{q}}^2} \frac{1}{\hat{q}_0^2} \right)^2 \frac{1}{4} \sin^2 q_0 \quad (\text{A.45})$$

Using identity (A.13) and setting $a, b = 0$

$$Q_1(0) = \frac{N_c}{L_s^2 L_0} \sum_{\vec{k}, k_0 \neq 0} \sum_{ij=1}^{D-1} \left(\frac{i}{\sqrt{2c_f}} \right)^2 \left(\frac{1}{\hat{q}^2} \left(\delta_{ij} - \frac{\hat{q}_i \hat{q}_j}{\hat{\mathbf{q}}^2} \right) + \frac{\hat{q}_i \hat{q}_j}{\hat{\mathbf{q}}^2} \frac{1}{\hat{q}_0^2} \right)^2 \frac{1}{4} \sin^2 q_0 \quad (\text{A.46})$$

$$\begin{aligned} &= -\frac{N_c}{2L_s^2 L_0} \sum_{\vec{q}, q_0 \neq 0} \sum_{ij=1}^{D-1} \frac{(\hat{q}_i \hat{q}_j + \delta_{ij} \hat{q}_0^2)^2}{(\hat{q}^2 + \hat{q}_0^2)^2} \frac{1}{\hat{q}_0^4} \frac{1}{4} \sin^2 q_0 \\ &= -\frac{N_c}{2L_s^2 L_0} \sum_{\vec{q}, q_0 \neq 0} \frac{1}{4} \sin^2 q_0 \sum_{ij=1}^{D-1} \frac{q_i^2 q_j^2 + 2q_i q_j \delta_{ij} q_0^2 + \delta_{ij}^2 q_0^4}{(\hat{q}^2 + \hat{q}_0^2)^2 \hat{q}_0^4} \\ &= -\frac{N_c}{2L_s^2 L_0} \sum_{\vec{q}, q_0 \neq 0} \frac{4c_0^2}{\hat{q}_0^2} + 2 \frac{N_c}{L^2 L_0} \sum_{\vec{q}, q_0 \neq 0} \frac{c_0^2 q_0^2}{(\hat{q}^2 + \hat{q}_0^2)^2} \\ &= -2 \frac{N_c}{L_s^2 L_0} \sum_{\vec{q}, q_0 \neq 0} \frac{c_0^2 q_0^2}{(\hat{q}^2 + \hat{q}_0^2)^2} - \frac{N_c}{L_0} \sum_{q_0 \neq 0} \frac{2}{\hat{q}_0^2} + \frac{N_c (L_0 - 1)}{2L_0} \quad (\text{A.47}) \end{aligned}$$

Second diagram

Now let us calculate the second diagram on (Fig.A.1, right). For Feynman rules see [46]

$$\begin{aligned} Q_2(0) &= \frac{N_c}{L^2 L_0} \sum_{k'_0 \neq 0, k'} \left(\frac{1}{2c_f} \right) D_{\rho\tau}^{cc}(k') 2 \sum_e f_{mce} f_{cne} \left[\begin{array}{c} \delta_{0\tau} \delta_{0\rho} c_{k'_\rho} c_{k'_0} + \delta_{\rho\tau} c_{2k'_0} - \frac{1}{6} \delta_{0\tau} k'_0 k'_\rho \\ -\frac{1}{6} \delta_{0\rho} k'_0 k'_\tau + \frac{1}{12} \delta_{0\tau} \delta_{0\rho} (k')^2 \end{array} \right] = \\ &= \frac{N_c}{L^2 L_0} \sum_{k'_0 \neq 0, k'} D_{\rho\rho}^{cc}(k') c_{2k'_0} \equiv \frac{N_c}{L^2 L_0} \sum_{k_0 \neq 0, k} D_{\rho\rho}^{cc}(k) c_{2k_0} \quad (\text{A.48}) \end{aligned}$$

$$c_{2k_0} = \cos k_0 = \cos^2 \frac{k_0}{2} - \sin^2 \frac{k_0}{2} = 1 - 2 \sin^2 \frac{k_0}{2} = 1 - \frac{1}{2} k_0^2 \quad (\text{A.49})$$

$$\begin{aligned} Q_2(0) &= -\frac{N_c}{L^2 L_0} \sum_{k, k_0 \neq 0} \frac{1}{2} + \frac{N_c}{L^2 L_0} \sum_{k, k_0 \neq 0} \frac{1 - \frac{1}{2} k_0^2}{\hat{k}^2 + \hat{k}_0^2} + \frac{N_c}{L^2 L_0} \sum_{k, k_0 \neq 0} \frac{1}{\hat{k}_0^2} \\ &= \frac{N_c}{L^2 L_0} \sum_{k, k_0 \neq 0} \frac{1 - \frac{1}{2} \hat{k}_0^2}{\hat{k}^2 + \hat{k}_0^2} + \frac{N_c}{L_0} \sum_{k_0 \neq 0} \frac{1}{\hat{k}_0^2} - \frac{1}{2} \frac{N_c}{L_0} (L_0 - 1) \quad (\text{A.50}) \end{aligned}$$

In addition to these two diagrams we need the corresponding ghost diagrams and the diagram for the measure. All of such were calculated as in [29] and amount to the term

$$Q_0 = \frac{N_c}{L_0} \sum_{k_0 \neq 0} \frac{1}{\hat{k}_0^2} \quad (\text{A.51})$$

Adding all these we get $\tilde{\Pi}_{00}^{ns}$

$$\tilde{\Pi}_{00}^{ns}(0) = \frac{3}{L_0 L_s^2} \sum_{k_0 \neq 0} \sum_k \left\{ \frac{2c_{k_0}^2 \hat{k}_0^2}{(\hat{k}^2 + \hat{k}_0^2)^2} - \frac{1 - \hat{k}_0^2/2}{\hat{k}^2 + \hat{k}_0^2} \right\} \quad (\text{A.52})$$

$$\tilde{\Pi}_{00}^{ns}(0) = \frac{3}{L_0 L_s^2} \sum_{k_0 \neq 0} \sum_{k_1, k_2} \left\{ \frac{2 \cos^2 \frac{k_0}{2} 4 \sin^2 \frac{\hat{k}_0}{2}}{(\cos^2 k_1 + \cos^2 k_2 + \cos^2 k_0)^2} - \frac{1 - 2 \sin^2 \frac{\hat{k}_0}{2}}{\cos^2 k_1 + \cos^2 k_2 + \cos^2 k_0} \right\} \quad (\text{A.53})$$

The infinite volume limit is obtained by replacement

$$\left(\frac{2\pi}{L_s} \right)^2 \sum_{\vec{k}} \rightarrow \int_{-\pi}^{\pi} d^2 k \quad (\text{A.54})$$

$$\tilde{\Pi}_{00}^{ns}(0) = \frac{3}{L_0} \sum_{k_0 \neq 0} \int_{-\pi}^{\pi} \frac{d^2 k}{4\pi^2} \left\{ \frac{8 \cos^2 \frac{k_0}{2} \sin^2 \frac{\hat{k}_0}{2}}{(\cos^2 k_1 + \cos^2 k_2 + \cos^2 k_0)^2} - \frac{1 - 2 \sin^2 \frac{\hat{k}_0}{2}}{\cos^2 k_1 + \cos^2 k_2 + \cos^2 k_0} \right\} \quad (\text{A.55})$$

We define the following

$$t = \sin^2 \left(\frac{\pi n_0}{L_0} \right)$$

$$S(t) = \frac{1}{4\pi^2} \int_{-\pi}^{\pi} \frac{dk_1 dk_2}{2(1+t) - \cos(k_1) - \cos(k_2)}$$

and $\tilde{\Pi}_{00}^{ns}$ can be presented in the more convenient for the practical calculation form

$$\tilde{\Pi}_{00}^{ns}(0) = \frac{3}{L_0} \sum_{n_0=1}^{L_0-1} \left(-\frac{1}{2} (1-2t) S(t) - t(1-t) \frac{2S(t)}{dt} \right), \quad t = \sin^2 \left(\frac{\pi n_0}{L_0} \right) \quad (\text{A.56})$$

In a more compact way it can be expressed as

$$W \equiv \tilde{\Pi}_{00}^{ns}(0) = -\frac{3}{L_0} \sum_{n_0=1}^{L_0-1} \frac{d}{dx} G(x), \quad x = \frac{\pi n_0}{L_0}, \quad (\text{A.57})$$

$$G(x) \equiv \sin x \cos x S(\sin^2 x) \quad (\text{A.58})$$

In the integral defining S we replace the inverse denominator in a following way

$$S(t) = \int_{-\pi}^{\pi} dk_1 dk_2 \int_0^{\infty} dy \exp[-y(2(1+t) - \cos k_1 - \cos k_2)] \quad (\text{A.59})$$

and identify two modified Bessel functions I_0 to get

$$S(t) = \int_0^{\infty} dy \exp[-y(2(1+t))] I_0^2(y). \quad (\text{A.60})$$

This can be expressed via hyper-geometric function [42] as

$$S(t) = \frac{(-z)^{1/2}}{2} F(1/2; 1/2; 1; z), \quad z = \frac{1}{t(t+2)}.$$

This ansatz relates the behaviour of $S(t)$ at low t to that of F at large negative z . Using [42] again one finds

$$S(t) = \frac{1}{2\pi^2} \sum_{n=0}^{\infty} \left[\frac{\Gamma(n+1/2)}{\Gamma(n+1)} \right]^2 z^{-n} [\log(-z) + 2\Psi(n+1) - 2\Psi(n+1/2)] \quad (\text{A.61})$$

A first approximation W_0 to W is obtained from the standard relationship between a sum and an integral:

$$W_0 = \frac{L_0}{2\pi} \int_{\pi/L_0}^{\pi-\pi/L_0} dG(x) + \frac{1}{4} \left[\frac{dG(x)}{dx} \Big|_{x=\frac{\pi}{L_0}} + \frac{dG(x)}{dx} \Big|_{x=\pi-\frac{\pi}{L_0}} \right] \quad (\text{A.62})$$

$$= -\frac{L_0}{\pi} G\left(\frac{\pi}{L_0}\right) + \frac{1}{2} \frac{dG(x)}{dx} \Big|_{x=\frac{\pi}{L_0}}, \quad (\text{A.63})$$

where use has been made of the symmetry of $\frac{dG(x)}{dx}$ under $x \leftrightarrow \pi - x$. Up to terms which vanish as $\pi/L_0 \rightarrow 0$, Eq. (A.61) gives:

$$W_0 \simeq -\frac{1}{2\pi} \left[\frac{3 \log 2}{2} + 1 - \log \pi + \log L_0 \right].$$

For that part of $G(x)$ which is analytic at $x = 0$, this is the right answer. A correction to the constant term in L_0 however arises from the logarithmic singularity of $G(x)$ (Euler-Mac-Laurin formula, [42]). As $x \rightarrow 0$, we have $\frac{dG}{dx} \simeq -\frac{1}{\pi} \log \frac{n_0}{L_0}$ up to analytic terms, whose contribution W^{log} to W from Eq. (A.61) can be computed using

$$\sum_{n_0=1}^{L_0/2} \log \frac{n_0}{L_0} = \log \left(\frac{(L_0/2)!}{L_0^{L_0/2}} \right) \simeq \log \frac{\sqrt{\pi L_0}}{(2e)^{L_0/2}}$$

and found to be

$$W^{log} = -\frac{1}{2\pi} [\log(2L_0\pi) - L_0(1 + \log 2)].$$

This we compare to the contribution W_0^{log} to W_0 of the same singular part of $\frac{dG}{dx}$, namely

$$W_0^{log} = -\frac{1}{2\pi} [\log(2L_0) - L_0(1 + \log 2)],$$

so that in the limit $L_0 \rightarrow \infty$ the final result is

$$W = W_0 - W_0^{log} + W^{log} \tag{A.64}$$

$$= -\frac{1}{2\pi} \left[\frac{5}{2} \log 2 - 1 + \log L_0 \right]. \tag{A.65}$$

A.4 Free field theory

We present here a solution of the free-field theory, used in Chapter 2 for checking simulation validity for the Higgs sector of the 2D model. Statistical sum is

$$Z_0 = \int e^{S_0} \quad (\text{A.66})$$

with action being

$$S_0 = -\frac{\beta}{N} \sum_x \left(\sum_{i=1}^2 \text{Tr} A_0(x) A_0(x + \hat{i}) - 2 \text{Tr} A_0^2(x) - \frac{h}{2} \text{Tr} A_0^2(x) \right) \quad (\text{A.67})$$

$$x = (i, j) \quad i = 0, \dots, n_x - 1, \quad j = 0, \dots, n_y - 1, \quad (\text{A.68})$$

Fields belong to the $SU(3)$ algebra and can be expressed via generators

$$A_0(x) = i \sum_a A_0^a T^a, \quad A_0^a(x) \text{ real} \quad (\text{A.69})$$

Using the tracelessness of the generators, we get

$$\text{Tr} A_0(x) A_0(y) = -\frac{1}{2} \sum_a A_0^a(x) A_0^a(y) \quad (\text{A.70})$$

We may rewrite the action in the following form

$$S_0 = \frac{1}{2} \frac{\beta}{N} \sum_a \sum_x \left(\sum_{i=1}^2 A_0^a(x) A_0^a(x + \hat{i}) - 2 A_0^a(x)^2 - \frac{h}{2} A_0(x)^2 \right) \quad (\text{A.71})$$

$$= -\frac{1}{4} \frac{\beta}{N} \sum_a \sum_x \left(\sum_{i=1}^2 (A_0^a(x) - A_0^a(x + \hat{i}))^2 + h A_0(x)^2 \right) \quad (\text{A.72})$$

and diagonalize it using the Fourier transform:

$$A(x) = \frac{1}{n_x n_y} \sum_k A(k) e^{ik \cdot x} \quad (\text{A.73})$$

$$k = \left(\frac{2\pi}{n_x} q, \frac{2\pi}{n_y} r \right) \quad q(r) = 0, \dots, n_x(n_y) \quad (\text{A.74})$$

In Fourier space

$$\sum_x A(x)^2 = \frac{1}{n_x n_y} \sum_k |A(k)|^2 \quad (\text{A.75})$$

$$\sum_x (A(x + \hat{i}) - A(x))^2 = \frac{1}{n_x^2 n_y^2} \sum_x \sum_{k, k'} A(k) (e^{ik \cdot \hat{i}} - 1) e^{ik \cdot x} A(k') (e^{ik' \cdot \hat{i}} - 1) e^{ik' \cdot x} \sum_x e^{i(k+k') \cdot x} = n_x n_y \delta_{k, -k'} \quad (\text{A.76})$$

$$A(-k) = \bar{A}(k), \quad -k = 2\pi - k \quad (\text{A.77})$$

$$\begin{aligned} \sum_x (A(x + \hat{i}) - A(x))^2 &= \frac{1}{n_x n_y} \sum_k |A(k)|^2 (e^{ik \cdot \hat{i}} - 1) (e^{-ik' \cdot \hat{i}} - 1) \\ &= \frac{2}{n_x n_y} \sum_k |A(k)|^2 (1 - \cos(k \cdot \hat{i})) \end{aligned} \quad (\text{A.78})$$

$$S_0 = \frac{1}{n_x n_y} \sum_a \sum_k \left[-\frac{1}{2} \frac{\beta}{N} |A_0^a(k)|^2 \left(\sum_i (1 - \cos(k \cdot \hat{i})) + \frac{h}{2} \right) \right] \quad (\text{A.79})$$

We define

$$K_{mn} = \frac{1}{n_x n_y} \frac{\beta}{N} \left(\sum_i (1 - \cos(k \cdot \hat{i})) + \frac{h}{2} \right) \delta_{mn} \quad (\text{A.80})$$

and the action takes the final form

$$S_0 = \sum_a \sum_k \left[-\frac{1}{2} |A_0^a(k)|^2 K_{mn} \right] \quad (\text{A.81})$$

Taking the integral over the Higgs fields, we get

$$Z_0 = \prod_k \prod_a 2 \sqrt{\frac{\pi N}{\beta}} \left(\frac{1}{2 \sum_i (1 - \cos(k \cdot \hat{i})) + h} \right)^{\frac{1}{2}} \quad (\text{A.82})$$

We are interested in the following estimate:

$$\sum_x \langle \text{Tr} A_0^2(x) \rangle = \frac{2N}{\beta} \frac{\partial \log Z_0}{\partial h} \quad (\text{A.83})$$

$$\log Z_0 = -\frac{1}{2} (N^2 - 1) \left(\sum_k \log \left(2 \sum_i (1 - \cos(k \cdot \hat{i})) + h \right) + \frac{1}{2} V \log \beta \right) + \mathcal{C}$$

$$\begin{aligned}
\frac{\partial \log Z_0}{\partial h} &= -\frac{1}{2}(N^2 - 1) \sum_k \frac{1}{2 \sum_i (1 - \cos(k \cdot \hat{i})) + h} \\
&\quad - \frac{1}{2}(N^2 - 1) \sum_{q=0}^{n_x-1} \sum_{r=0}^{n_y-1} \frac{1}{2 \left(1 - \cos\left(\frac{2\pi}{n_x} q\right)\right) + 2 \left(1 - \cos\left(\frac{2\pi}{n_y} r\right)\right) + h} \\
\langle \text{Tr } A_0^2(x) \rangle &= -\frac{(N^2 - 1)N}{n_x n_y \beta} \sum_{q=0}^{n_x-1} \sum_{r=0}^{n_y-1} \frac{1}{2 \left(1 - \cos\left(\frac{2\pi}{n_x} q\right)\right) + 2 \left(1 - \cos\left(\frac{2\pi}{n_y} r\right)\right) + h} \\
&\hspace{15em} \text{(A.84)}
\end{aligned}$$

This quantity can be computed numerically for any given lattice and is very suitable to test the simulation of the Higgs sector of the model.

A.5 Weak field expansion for Polyakov loops

One may also test the measurement of the Polyakov loops correlations using the small field expansion

$$P_{0,x} = \langle \text{Tr} \exp(A_0(0) L_0) \text{Tr} \exp(A_0(x) L_0) \rangle \quad (\text{A.85})$$

$$P_{0,x} = \int \prod_x dA \text{Tr} \exp(A_0(0) L_0) \text{Tr} \exp(A_0(x) L_0) \exp S_0 \quad (\text{A.86})$$

We expand Polyakov loops, assuming that A_0 is small:

$$\exp(A_0(0) L_0) = I + A_0(0) L_0 + \frac{1}{2} A_0(0)^2 L_0^2 + \dots \quad (\text{A.87})$$

$$P_{0,x} = \left\langle \text{Tr} \left(I + A_0(0) L_0 + \frac{1}{2} A_0(0)^2 L_0^2 \right) \text{Tr} \left(I + A_0(x) L_0 + \frac{1}{2} A_0(x)^2 L_0^2 \right) \right\rangle \quad (\text{A.88})$$

$$= \langle \text{Tr} I \rangle + \frac{1}{2} L_0^2 \langle \text{Tr} (A_0(0)^2) \rangle + \frac{1}{2} L_0^2 \langle \text{Tr} (A_0(x)^2) \rangle \quad (\text{A.89})$$

$$+ \frac{1}{4} L_0^4 \langle \text{Tr} (A_0(0)^2) \text{Tr} (A_0(x)^2) \rangle \quad (\text{A.90})$$

$$\text{Tr} A_0(0) A_0(x) = -\frac{1}{2} \sum_i A_0^i(0) A_0^i(x) \quad (\text{A.91})$$

$$F(0,x) = \langle \text{Tr} (A_0(0)^2) \text{Tr} (A_0(x)^2) \rangle = -\frac{1}{4} \left\langle \sum_a A_0^a(0)^2 \sum_b A_0^b(x)^2 \right\rangle \quad (\text{A.92})$$

To calculate such correlation function we proceed in a standard manner, introducing the sources in the action

$$S[J] = -\frac{1}{2} \frac{\beta}{N} \frac{1}{n_x n_y} \sum_k \left(\sum_{a,b} A_0^a(k) \Delta_{ab}^{-1}(k) A_0^b(-k) - \sum_a \frac{\beta}{N} \frac{1}{n_x n_y} \text{Re} J^a(k) \bar{A}_0^a(k) \right) \quad (\text{A.93})$$

with

$$\Delta_{ab}(k) = ((1 - \cos(k \cdot \hat{i})) + h)^{-1} \delta_{a,b} \quad (\text{A.94})$$

New partition function is

$$Z[J] = Z_0 \exp \left(\frac{1}{2} \frac{\beta}{N} \frac{1}{n_x n_y} \sum_k \sum_{a,b} J^a(k) \Delta_{ab}(k) J^b(-k) \right) \quad (\text{A.95})$$

and the required correlation can be calculated taking the derivatives with respect to the sources and then setting them to zero

$$\begin{aligned}
F(0, x) &= -\frac{1}{4} \left(\frac{1}{n_x n_y} \right)^2 \sum_{a,b,p,p'} \exp(ip'R) (A_0^a(p))^2 (A_0^b(p'))^2 \\
&\quad \times \exp \left(\frac{1}{2} \frac{\beta}{N} \frac{1}{n_x n_y} \sum_k \sum_{a,b} J^a(k) \Delta_{ab}(k) J^b(-k) \right) \\
&= -\frac{1}{4} \left(\frac{1}{n_x n_y} \right)^2 \sum_{c,d,p,p'} \exp(ip'R) \\
&\quad \times \frac{\partial^2}{J^c(p')^2} \frac{\partial^2}{J^d(p)^2} \exp \left(\frac{1}{2} \frac{\beta}{N} \frac{1}{n_x n_y} \sum_k \sum_{a,b} J^a(k) \Delta_{ab}(k) J^b(-k) \right)
\end{aligned}$$

$$F(0, x) = -\frac{\beta^2}{4N^2 (n_x n_y)^4} \sum_{c,d,p,p'} \exp(ip'R) \left[(\Delta_{cc}(p')) (\Delta_{dd}(p)) + \delta_{p,p'} (2\Delta_{cd}(p'))^2 \right] \tag{A.96}$$

A.6 Factorization of Matterfields

First, we have to derive some identities which will be used to prove the factorization of the higher-order averages. Let A be an arbitrary matrix belonging to the $SU(3)$ algebra. Such matrix can always be transformed to the diagonal form. Then on diagonal will be its eigenvalues, which we will call γ_1 , γ_2 and γ_3 . Tracelessness implies $\gamma_3 = -\gamma_1 - \gamma_2$. Our consideration [59] is based on the general expression for the determinant

$$\log \text{Det}(1 - tA) = \text{Tr} \log(1 - tA) \quad (\text{A.97})$$

Let us calculate the left-hand side of it:

$$\begin{aligned} \text{Det}(1 - tA) &= (1 - t\gamma_1)(1 - t\gamma_2)(1 + t(\gamma_1 + \gamma_2)) \\ &= 1 - t^2(\gamma_1^2 + \gamma_2^2 + \gamma_1\gamma_2) + t^3(\gamma_1^2\gamma_2 + \gamma_1\gamma_2^2) \end{aligned}$$

The quantities which we are looking for are:

$$\begin{aligned} A_2 &\equiv \text{Tr}A^2 = \gamma_1^2 + \gamma_2^2 + (\gamma_1 + \gamma_2)^2 \\ &= 2(\gamma_1^2 + \gamma_2^2 + \gamma_1\gamma_2) \end{aligned}$$

$$\begin{aligned} A_3 &\equiv \text{Tr}A^3 = \gamma_1^3 + \gamma_2^3 - (\gamma_1 + \gamma_2)^3 = \\ &= -3(\gamma_1^2\gamma_2 + \gamma_1\gamma_2^2) \end{aligned}$$

and we have

$$\text{Det}(1 - tA) = 1 - \frac{A_2}{2}t^2 - \frac{A_3}{3}t^3$$

Now we shall expand logarithms on the both sides of the identity. As long as this expansion should be valid for arbitrary values of t , we can match the coefficients near any power of it. Left-hand side:

$$\ln \text{Det}(1 - tA) = -\frac{1}{2}A_2t^2 - \frac{1}{3}A_3t^3 - \frac{1}{8}A_2^2t^4 - \frac{1}{6}A_2A_3t^5 - \frac{1}{18}A_3^2t^6 - \frac{1}{24}A_2^3t^6 + O(t^7)$$

Right-hand side:

$$\text{Tr} \log(1 - tA) = -\frac{1}{2}t^2 \text{Tr}A^2 - \frac{1}{3}t^3 \text{Tr}A^3 - \frac{1}{4}t^4 \text{Tr}A^4 - \frac{1}{5}t^5 \text{Tr}A^5 - \frac{1}{6}t^6 \text{Tr}A^6 + O(t^7)$$

and we immediately get:

$$A_2^2 = 2\text{Tr}A^4 \quad (\text{A.98})$$

$$\frac{5}{6}A_2A_3 = \text{Tr}A^5 \quad (\text{A.99})$$

$$\frac{1}{3}A_3^2 + \frac{1}{4}A_2^3 = Tr A^6 \quad (\text{A.100})$$

Mean Field Calculation for A_{22} :

Here we will work within the mean field approximation:

$$A_\alpha(x)A_\beta(x) \rightarrow \frac{1}{4}\delta_{\alpha\beta}A_2(x)$$

$$2A_4(x) = \frac{1}{2^2} \sum A_\alpha(x)A_\alpha(x)A_\beta(x)A_\beta(x)$$

Using Wick's theorem we get:

$$\begin{aligned} \langle 2A_4(x) \rangle &= \frac{1}{2^2} \sum_{\alpha,\beta} \langle A_\alpha(x)A_\alpha(x)A_\beta(x)A_\beta(x) \rangle = \frac{1}{2^2} \sum_{\alpha,\beta} \langle A_\alpha(x)A_\alpha(x) \rangle \langle A_\beta(x)A_\beta(x) \rangle \\ &+ \frac{1}{2^2} 2 \sum_{\alpha,\beta} \langle A_\alpha(x)A_\beta(x) \rangle \langle A_\alpha(x)A_\beta(x) \rangle \\ &= \frac{1}{2^2} \left(\sum_\alpha \frac{1}{4}\delta_{\alpha\alpha}A_2(x) \right)^2 + \frac{1}{2^2} 2 \sum_{\alpha,\beta} \left(\frac{1}{4}\delta_{\alpha\beta}A_2(x) \right)^2 \\ &= \frac{1}{2^2} \left(8\frac{1}{4}A_2 \right)^2 + \frac{1}{2^2} 2 * 8 \left(\frac{1}{4}A_2 \right)^2 = \frac{5}{4}A_2^2 \end{aligned}$$

$$\langle A_n(x) A_m(0) \rangle = A_{nm}(x) + \langle A_n(x) \rangle \langle A_m(x) \rangle$$

And we arrive to the final result

$$\langle A_2^2(x) \rangle = A_{2,2}(0) + A_2^2$$

Calculation of A_{33}

$$\langle A_3(x) A_3(0) \rangle = A_{33}(x) + \langle A_3(x) \rangle \langle A_3(x) \rangle$$

In our phase

$$\langle A_3(x) \rangle = 0 \quad (\text{A.101})$$

so

$$A_{33}(0) = \langle A_3(x)^2 \rangle$$

$$Tr A^3 = \sum_{ijk} A_i A_j A_k Tr T_i T_j T_k = \sum_{ijk} A_i A_j A_k \frac{1}{4} (d_{ijk} + i f_{ijk}) = \frac{1}{4} \sum_{ijk} d_{ijk} A_i A_j A_k$$

where we used the antisymmetric properties of f_{ijk} .

$$\langle Tr A^3 Tr A^3 \rangle = \frac{1}{4} \frac{1}{4} \sum_{ijk} \sum_{lmn} d_{ijk} d_{lmn} A_i A_j A_k A_l A_m A_n$$

Now we will use the property of d - it being zero after contraction when two indices are the same and its symmetry which leaves us only with six equal terms

$$\langle Tr A^3 \rangle = \frac{1}{4} \frac{1}{4} \left(\frac{1}{4} A_2 \right)^3 * \sum_{ijk} d_{ijk} d_{ijk} = \frac{1}{4} \frac{1}{4} \left(\frac{1}{4} A_2 \right)^3 6 \frac{N^2 - 4}{N} (N^2 - 1) = \frac{5}{64} A_2^3$$

$$\langle Tr A^3 \rangle = \frac{5}{64} A_2^3$$

Or

$$A_{33}(0) = \frac{5}{64} A_2^3$$

Calculation of $\langle A_2 A_3 \rangle$

$$\begin{aligned} \langle A_2 A_3 \rangle &= \left\langle \frac{1}{2} \frac{1}{4} \sum_n \sum_{ijk} A_n A_n A_i A_j A_k d_{ijk} \right\rangle = \\ &= \frac{1}{2} \frac{1}{4} 3 \sum_n \sum_{ijk} \langle A_n A_n A_i \rangle \langle A_j A_k \rangle d_{ijk} + \\ &+ \frac{1}{2} \frac{1}{4} 6 \sum_n \sum_{ijk} \langle A_n A_i A_j \rangle \langle A_n A_k \rangle d_{ijk} + \\ &+ \frac{1}{2} \frac{1}{4} \sum_n \sum_{ijk} \langle A_n A_n \rangle \langle A_i A_j A_k \rangle d_{ijk} \end{aligned}$$

$$\begin{aligned} \langle A_2 A_3 \rangle &= \\ &= \frac{1}{2} \frac{1}{4} 3 \sum_n \sum_{ijk} \langle A_n A_n A_i \rangle \frac{1}{4} A_2 \delta_{jk} d_{ijk} + \\ &+ \frac{1}{2} \frac{1}{4} 6 \sum_n \sum_{ijk} \langle A_n A_i A_j \rangle \frac{1}{4} A_2 \delta_{nk} d_{ijk} + \\ &+ \frac{1}{2} \frac{1}{4} \sum_n \sum_{ijk} \frac{1}{4} A_2 \langle A_i A_j A_k \rangle d_{ijk} \end{aligned}$$

The first term falls out completely - contraction of d with two equal indices.

$$\begin{aligned} \langle A_2 A_3 \rangle &= \frac{1}{2} \frac{1}{4} 6 \sum_n \sum_{ijk} d_{ijk} \delta_{nk} \langle A_n A_i A_j \rangle \frac{1}{4} A_2 + \\ &+ \frac{1}{2} \frac{1}{4} \sum_n \sum_{ijk} \frac{1}{4} d_{ijk} A_2 \langle A_i A_j A_k \rangle \end{aligned}$$

Summing over n :

$$\begin{aligned}\langle A_2 A_3 \rangle &= \frac{1}{2} \frac{1}{4} 6 \frac{1}{4} A_2 \sum_{ijk} d_{ijk} \langle A_k A_i A_j \rangle + \frac{1}{2} \frac{1}{4} 8 \frac{1}{4} A_2 \sum_{ijk} d_{ijk} \langle A_i A_j A_k \rangle = \\ &= \frac{1}{2} \frac{1}{4} (6 + 8) \frac{1}{4} A_2 \sum_{ijk} d_{ijk} \langle A_k A_i A_j \rangle = \frac{1}{2} \frac{1}{4} (6 + 8) A_2 A_3 = \frac{7}{4} A_2 A_3\end{aligned}$$

Correlation Functions

Now we turn to the correlation functions. Square brackets denote contraction and we will silently use the formulae above.

$$\langle A_n(x) A_m(0) \rangle = A_{nm}(x) + \langle A_n(x) \rangle \langle A_m(x) \rangle$$

$$\begin{aligned} A_{24}(R) &= \langle A_2(R); A_4(0) \rangle = \frac{1}{2} \langle A_2(R); A_2^2(0) \rangle = \\ &= \frac{1}{2} \left[\left[A_2(R); \frac{N^2+1}{N^2-1} A_2^2(0) \right] \right] = \frac{1}{2} 2 \frac{N^2+1}{N^2-1} [[A_2(R); A_2(0)]] [[A_2(0)]] = \\ &= \frac{N^2+1}{N^2-1} A_{22}(R) A_2 = \frac{5}{4} A_{22}(R) A_2 \end{aligned}$$

$$\begin{aligned} A_{35}(R) &= \langle A_3(R); A_5(0) \rangle = \frac{5}{6} \langle A_3(R); A_3(0) A_2(0) \rangle = \\ &= \frac{5}{6} [[\langle A_3(R) \rangle]; \langle A_3(0) A_2(0) \rangle]] = \\ &= \frac{5}{6} \frac{N^2+5}{N^2-1} [[\langle A_3(R) \rangle]; \langle A_3(0) \rangle \langle A_2(0) \rangle]] = \\ &= \frac{5}{6} \frac{N^2+5}{N^2-1} ([[A_3(R); A_3(0)]] [[A_2(0)]] + [[A_3(R); A_2(0)]] [[A_3(0)]]) = \\ &= \frac{35}{24} A_{3,3} A_2 \end{aligned}$$

$$\begin{aligned} A_{44}(R) &= \langle A_4(R); A_4(0) \rangle = [[\langle A_4(R) \rangle]; \langle A_2^2(0) \rangle]] = \\ &= \left(\frac{1}{2} \frac{N^2+1}{N^2-1} \right)^2 [[A_2^2(R); A_2^2(0)]] = \\ &= \left(\frac{1}{2} \frac{N^2+1}{N^2-1} \right)^2 \left(2 [[A_2(R); A_2(0)]] [[A_2(R); A_2(0)]] + 4 [[A_2(R); A_2(0)]] [[A_2(0)]]^2 \right) = \\ &= \left(\frac{1}{2} \frac{N^2+1}{N^2-1} \right)^2 (2A_{22}(R)^2 + 4A_{22}(R) A_2^2) = \\ &= \left(\frac{5}{8} \right)^2 (2A_{22}(R)^2 + 4A_{22}(R) A_2^2) \end{aligned}$$

$$\begin{aligned}
A_{55}(R) &= \langle A_5(R); A_5(0) \rangle = [[\langle A_5(R) \rangle]; \langle A_5(0) \rangle] = \\
&= \left(\frac{5}{6}\right)^2 \left(\frac{N^2+5}{N^2-1}\right)^2 [[A_2(R) A_3(R); A_2(0) A_3(0)]] = \\
&= \left(\frac{5}{6}\right)^2 \left(\frac{N^2+5}{N^2-1}\right)^2 \left(\begin{aligned} & [[A_2(R); A_2(0)]][[A_3(R); A_3(0)]] + \\ & + [[A_2(R); A_3(0)]]^2 + \\ & + [[A_2(R); A_2(0)]][[A_3(R)]]^2 + \\ & + 2[[A_2(R); A_3(0)]][[A_3(R)]][[A_2(R)]] + \\ & + [[A_3(R); A_3(0)]][[A_2(R)]]^2 \end{aligned} \right) = \\
&= \left(\frac{5}{6}\right)^2 \left(\frac{N^2+5}{N^2-1}\right)^2 (A_{22}A_{33} + A_{23}^2 + A_{22}A_3^2 + 2A_{23}A_3A_2 + A_{33}A_2^2) = \\
&= \left(\frac{5}{6}\right)^2 \left(\frac{N^2+5}{N^2-1}\right)^2 (A_{22}A_{33} + A_{33}A_2^2) = \left(\frac{35}{24}\right)^2 (A_{22}A_{33} + A_{33}A_2^2)
\end{aligned}$$

In the last step we used the symmetry relation (A.101)

Bibliography

- [1] P. Bialas, A. Morel, B. Petersson, K. Petrov and T. Reisz, “High Temperature 3D QCD: Dimensional Reduction at Work”, *Nucl. Phys.* **B581** (2000) 477.
- [2] P. Bialas, A. Morel, B. Petersson, K. Petrov and T. Reisz, “ QCD with Adjoint Scalars in 2D: Properties in the Colourless Scalar Sector ”, *Nucl. Phys.* **B603** (2001) 369.
- [3] P. Bialas, A. Morel, B. Petersson, K. Petrov and T. Reisz, “Screening Masses in Dimensionally Reduced (2+1)D Gauge Theory”, *Nucl.Phys.Proc.Suppl.* (**2002**) 882-884.
- [4] P. Bialas, A. Morel, B. Petersson, K. Petrov and T. Reisz, “Z(3) Symmetric Dimensional Reduction of (2+1)D QCD”, submitted to *Nucl. Phys. Proc. Suppl.*
- [5] F.Karsch, “Lattice QCD at High Temperature and Density”, hep-lat/0106019
- [6] G. Boyd, J. Engels, F. Karsch, E. Laermann, C. Legeland, M. Lütgemeier, B. Petersson, *Phys.Rev.Lett.* 75 (1995) 4169-4172
- [7] P. Ginsparg, *Nucl. Phys.* **B170** (1980) 388.
- [8] T. Appelquist and R. Pisarski, *Phys. Rev.* **D23** (1981) 2305.
- [9] S. Nadkarni, *Phys. Rev.* **D27** (1983) 917; *Phys. Rev.* **D38** (1988) 3287.
- [10] N. P. Landsman, *Nucl. Phys.* **B322** (1989) 498.
- [11] T. Reisz, *Z. f. Phys.* **C53** (1992) 169.
- [12] J. Engels, F. Karsch, E. Laermann, C. Legeland, M. Lütgemeier, B. Petersson, T. Scheideler, *Nucl.Phys.Proc.Suppl.***53**:420-422,1997

- [13] J.Engels, Nucl.Phys. **B30** (1993), 347
- [14] P. Lacock, D. E. Miller and T. Reisz, *Nucl. Phys.* **B369** (1992) 501.
- [15] L. Kärkkäinen, P. Lacock, D. E. Miller, B. Petersson and T. Reisz, *Phys. Lett.* **B282** (1992) 121.
- [16] L. Kärkkäinen, P. Lacock, B. Petersson and T. Reisz, *Nucl. Phys.* **B395** (1993) 733.
- [17] P. Lacock, T. Reisz, *Nucl. Phys. B (Proc. Suppl.)* **30** (1993) 307
- [18] K. Kajantie, M. Laine, K. Rummukainen, M. Shaposhnikov, *Phys. Lett* **77** (1996) 2887, *Nucl. Phys.* **B493** (1997) 413.
M. Gurtler, E.-M. Ilgenfritz, A. Schiller, *Phys. Rev.* **D56** (1997) 3888.
F. Karsch, T. Neuhaus, A. Patkos, J. Rank, *Nucl. Phys. Proc. Supl.* **53** (1997) 623.
- [19] K. Kajantie, M. Laine, K. Rummukainen, M. Shaposhnikov, *Nucl. Phys.* **B503** (1997) 357.
- [20] K. Kajantie, M. Laine, A. Rajantie, K. Rummukainen, and M. Tsypin, *JHEP* **9811** (1998) 11.
- [21] K. Kajantie, M. Laine, J. Peisa, A. Rajantie, K. Rummukainen, M. Shaposhnikov *Phys. Rev. Lett.* **79** (1997) 3130.
- [22] S. Datta, S. Gupta, Nucl. Phys. **B534** (1998) 392, *Phys.Lett.* **B471** (2000) 382.
- [23] F. Karsch, M. Oevers and P. Petreczky, “Screening masses of hot $SU(2)$ gauge theory from the 3D adjoint Higgs model”, hep-ph/9902373.
- [24] A. Hart and O. Philipsen, “The spectrum of the three-dimensional adjoint Higgs model and hot $SU(2)$ gauge theory,” , hep-lat/9908041.
- [25] L. Kärkkäinen, P. Lacock, D.E. Miller, B. Petersson, T. Reisz *Phys. Lett.* **B312** (1993) 173.
- [26] G.S. Bali, J. Fingberg, U.M. Heller, F. Karsch and K. Schilling, *Phys. Rev. Lett.* **71** (1993) 3059
F. Karsch, E. Laermann, M. Lütgemeier *Phys. Lett.* B346 (1995) 94.
- [27] E. D’Hoker, *Nucl. Phys* **B201** (1982) 401.

- [28] C. Legeland, *PhD. Thesis*, “*Aspects of (2+1) Dimensional Lattice Gauge Theory*” (University of Bielefeld, Germany, September 1998).
- [29] B. Petersson and T. Reisz, *Nucl. Phys.* **B353** (1991) 757.
- [30] C. Curci and P. Menotti, *Z. f. Phys.* **C21** (1984) 281; C. Curci, P. Menotti and G. Paffuti, *Z. f. Phys.* **C26** (1985) 549.
- [31] T. Reisz, *Jour. Math. Phys.* **32** (1991) 515
- [32] T. Reisz, In preparation
- [33] A. Irbäck, P. Lacock, D. Miller, B. Petersson, T. Reisz, *Nucl. Phys.* **B363** (1991) 34.
- [34] L. Kärkkäinen, P. Lacock, D.E. Miller, B. Petersson and T. Reisz, *Nucl. Phys.* **B418** (1994) 3.
- [35] T. Reisz, “Dimensionally Reduced SU(2) Yang-Mills Theory is Confined”, in *Quantum Field Theoretical Aspects of High Energy Physics*, 230-235, B. Geyer and E.M. Ilgenfritz Eds., Franckenhausen 1993.
- [36] M. Caselle, R. Fiore, F. Gliozzi, P. Guaita and S. Vinti, *Nucl. Phys. B* **422**, 397 (1994) [arXiv:hep-lat/9312056].
- [37] N. Cabibbo and E. Marinari, *Phys. Lett.* **B119** (1982) 387.
- [38] A. D. Kennedy and B. J. Pendleton, *Phys. Lett.* **B156** (1985) 393.
- [39] D. J. Gross and E. Witten, *Phys. Rev.* **D21** (1980) 446.
- [40] C. B. Lang, P. Salomonson and B. S. Skagerstam, *Phys. Letters* **100** (1981) 29.
- [41] I.S. Gradshteyn and I.M. Ryzhik, *Table of Integrals, Series, and Products*, Alan Jeffrey, Ed. (Academic Press).
- [42] M. Abramowitz and I.A. Stegun, *Handbook of Mathematical Functions*, (National Bureau of Standards).
- [43] M. Gao, *Phys. Rev.* **D40** (1989) 2708.
- [44] O. Kaczmarek, F. Karsch, E. Laermann and M. Lutgemeier, “*Heavy quark potentials in quenched QCD at high temperature*,” hep-lat/9908010.
- [45] T. Reisz, *Z. f. Phys.* **C53** (1992) 169.

- [46] H. Rothe, Introduction to Lattice Gauge Theories.
- [47] A. M. Ferrenberg, Robert H. Swendsen, *Phys.Rev.Lett.* **63** (1989) 1195-1198.
- [48] M.Creutz, Quarks, gluons and lattices, Cambridge University Press (1993)
- [49] L. Kärkkäinen, P. Lacock, D.E. Miller, B. Petersson and T. Reisz, *Phys. Lett.* **B282** (1992) 121.
- [50] L. Kärkkäinen, P. Lacock, B. Petersson and T. Reisz, *Nucl. Phys.* **B395** (1993) 733.
- [51] O. Philipsen, “Static correlation lengths in QCD at high temperature and finite density”, hep-lat/0011019.
- [52] P. Arnold and L.G. Yaffe, *Phys. Rev.* **D52** (1995) 7208.
- [53] A. Hart, O. Philipsen, J.D. Stack and M. Teper, *Phys. Lett.* **B396** (1997) 217.
- [54] A. Hart and O. Philipsen, *Nucl. Phys.* **B572** (2000) 243.
- [55] G. Parisi, *Statistical Field Theory* (Addison-Wesley, New York, 1988)
- [56] M. Alford and M. Gleiser *Phys. Rev* **D48** (1993) 2838; J. Borrill and M. Gleiser, *Nucl. Phys.* **B483** (1997) 416.
- [57] A.D. Martin and T.D. Spearman. Elementary Particle Theory. North-Holland Publishing Co., Amsterdam, 1970.
- [58] W. Buchmuller and O. Philipsen *Phys. Lett.* **B397** (1997) 112.
- [59] We thank M. Bauer for providing us with this simple trick.
- [60] R. Pisarski, “*Quark-Gluon Plasma as a condensate of SU(3) Wilson Lines*”, hep-ph/0006205. K. Kajantie, M. Laine, J. Peisa, A. Rajantie, K. Rummukainen, M. Shaposhnikov *Phys. Rev. Lett.* **79** (1997) 3130.
- [61] <http://etherboot.sourceforge.net/>
- [62] <http://www.lam-mpi.org>